Universiteit Utrecht

Master thesis

Surface states on Weyl metals

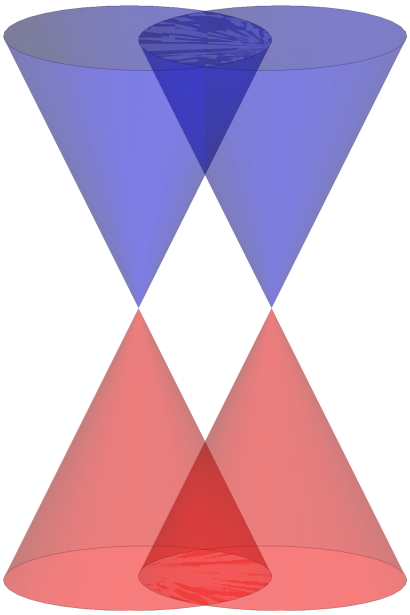

Author:
C.J.J. van Langen
Institute for Theoretical Physics
Utrecht University

Supervisors:
Prof. dr. ir. H.T.C. Stoof
Institute for Theoretical Physics
Utrecht University
and
E.C.I. van der Wurff, MSc.
Institute for Theoretical Physics
Utrecht University

June 25, 2018

Abstract

In this thesis we investigate the effect of a magnetic field on the surface states of a slab of Weyl semimetal surrounded by a vacuum. We consider a time reversal symmetry broken semimetal by splitting the Weyl cones up in momentum space. We warm up by calculating the Landau level states in the bulk for a magnetic field parallel and perpendicular to the direction in which the cones are split in momentum space. Next, we find the wavefunction in a half-infinite semimetal and match to the vacuum solutions. For zero magnetic field, we find gapless, chiral surface states with dispersion $E = -v_F k_y$, existing on a Fermi arc. For a magnetic field parallel to the surface, we find solutions using a WKB approximation. For magnetic fields perpendicular to the surface, we find no surface state solution in a half-infinite semimetal. Since Weyl metals have large anomalous magnetic moments [1], the surface states are altered by anomalous magnetic effects. We investigate the effect of the new anomalous terms on the surface states in a parallel magnetic field, and find that in some cases the surface states are altered. Since we found no surface states for a perpendicular magnetic field in the half-infinite Weyl metal, we switch to a finite slab of Weyl metal, and find that surface states are possible. Focussing on the high magnetic field limit, where only the lowest Landau level contributes, we find analytical solutions. Moreover, we find that closed magnetic orbits are possible due to the chiral lowest Landau level acting as a one-way "conveyor belt", carrying particles from one surface to the other. These orbits have discrete energy levels and depend on the length of the material and the Fermi velocity. We look at the influence of anomalous effects on these orbits and find that the Fermi velocity is rescaled and the energy is Zeeman shifted. Finally, using numerics, we find the first-order correction in B on the energy by adding one more Landau level.

Contents

Chapter 1

Introduction to Weyl semimetals

In 2010 the Nobel Prize in Physics was awarded to Andre Geim and Konstantin Novoselov for their work on graphene [2]. Graphene is a 2D layer with a thickness of one carbon atom, arranged on a honeycomb lattice. The honeycomb lattice is pictured in Figure 1.1. The lattice is divided into two sublattices A and B. The first Brillouin zone is a hexagon, with three atoms of each sublattice. It is clear that the points of the same sublattice are equivalent by the symmetry of the lattice, so we can consider only two corners of different sublattice. We label these points $\mathbf{K}, \mathbf{K}'$ and choose our coordinate system such that we have $\mathbf{K} = \left(4\pi/3\sqrt{3}a, 0\right)$ and $\mathbf{K}' = \left(-4\pi/3\sqrt{3}a, 0\right)$. These points are called the Dirac points. At these points, the conical conduction and valence bands of graphene intersect (see Figure 1.1). Close to the Dirac points $\mathbf{K}, \mathbf{K}'$, one can describe the electrons in the material by two 2D massless Dirac Hamiltonians

$$H_\chi = v_F \left(\chi k_x \tau_x + k_y \tau_y\right), \tag{1.1}$$

where v_F is the Fermi velocity, $\mathbf{k} = (k_x, k_y)$ is the wavevector relative to $\mathbf{K}$ and $\mathbf{K}'$, τ_x, τ_y are Pauli matrices and the chirality $\chi = 1$ for the cone at $\mathbf{K}$ and $\chi = -1$ for the cone at $\mathbf{K}'$. For zero chemical potential, the Fermi surface is zero-dimensional, located at the point of intersection of the conical bands. Thus, close to the Fermi surface, the system is described by a gapless linear dispersion $E \propto |\mathbf{k}|$. These conical dispersions are called Dirac cones.

Graphene has inversion symmetry, time-reversal symmetry and rotational symmetry along the six points of the hexagons. These symmetries prove to be very important for the electronic properties of graphene. The time-reversal operator complex conjugates and sends $t \to -t$, causing the direction of the momentum to be reversed, $\mathbf{k} \to -\mathbf{k}$. This sends $\mathbf{K}$ to $\mathbf{K}'$, exchanging the Dirac cones. The Hamiltonian 1.1 is time-reversal symmetric, as $H_1(\mathbf{k}) = H^\star_{-1}(-\mathbf{k})$ holds since $k_x\tau_x$ changes sign while $k_y\tau_y$ does not, as $\tau_y^\star = -\tau_y$. Note that time-reversal symmetry also reverses spin, but since the Pauli matrices τ represent the sublattice structure rather than the spin, we do not have to take this into account. Inversion symmetry sends $\mathbf{r} \to -\mathbf{r}$, giving $\mathbf{k} \to -\mathbf{k}$, also exchanging the Dirac cones. However, the sign of $k_y\tau_y$ is not switched back by this operation, which is needed to obtain $H_{-1}(\mathbf{k})$. Consequently, the inversion operator also requires a rotation τ_x, since $\tau_x\tau_y\tau_x = -\tau_y$, switching back the sign of $k_y\tau_y$ to obtain $H_{-1}(\mathbf{k})$. This rotation is needed because inversion also switches the sublattices.

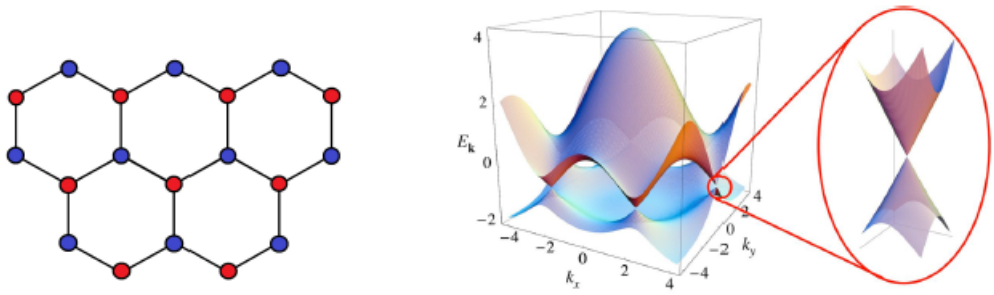

Figure 1.1 – The honeycomb lattice of graphene (left) and the corresponding band structure (right), taken from [3]. In the picture on the left, the two sublattice A and B are pictured in different colors. In the picture on the right six band-touching points (Dirac points) are shown. Around these points the electrons can be described by a 2D Dirac Hamiltonian with a linear energy spectrum.

The energies in graphene are given by

$$E = \pm\hbar v_F \sqrt{k_x^2 + k_y^2}. \tag{1.2}$$

Any perturbation of the form $m\tau_z$ opens up a gap, giving

$$E = \pm\hbar v_F \sqrt{k_x^2 + k_y^2 + m^2}.$$

This destroys the Dirac point at $\mathbf{k} = \mathbf{0}$, as $\mathbf{k} = \mathbf{0}$ is no longer a band crossing point and there is no other point satisfying $E = 0$. Such a perturbation would preserve time-reveral symmetry, but break inversion symmetry, as inversion sends $m\tau_z$ to $\tau_x m\tau_z\tau_x = -m\tau_z$. Therefore, the existence and stability of the Dirac points are protected by inversion symmetry.

Dirac and Weyl metals are like the three-dimensional cousins of graphene. They possess similar electronic properties and their low-energy electrons can be described by respectively the Dirac and Weyl equation, giving cone-like dispersions around the Fermi surface. A Dirac semimetal is defined as a 3D semimetal (since it has a zero-dimensional Fermi surface for zero chemical potential) which for low energies has quasiparticle excitations that obey the Dirac equation. Like graphene, a Dirac semimetal has time-reversal and inversion symmetry. A Weyl semimetal is made by taking a Dirac semimetal and breaking time-reversal and/or inversion symmetry. We describe the Weyl semimetal by two 3D Weyl Hamiltonians

$$H = \epsilon\hbar v_F(\mathbf{k} - \epsilon\mathbf{b}) \cdot \boldsymbol{\sigma} - \epsilon b_0, \tag{1.3}$$

describing two cones around the Weyl points (3D Dirac points, also called Weyl nodes) with chirality $\epsilon = \pm 1$, separated by the four-vector $\mathbf{b}_\mu = (b_0, \mathbf{b})$. The splitting vector $\mathbf{b}$ breaks time-reversal symmetry and b_0 breaks inversion symmetry. Note that in this case the Pauli matrices σ_i denote the spin structure rather than the sublattice structure. We have assumed that the system is isotropic, such that the Fermi velocity is equal in all directions. The chirality for massless particles indicates whether the momentum and spin of particles in a Weyl cone

are parallel or anti-parallel in the positive energy band. The Hamiltonian 1.3 resembles the Hamiltonian 1.1 of two Dirac cones in graphene. They both describe two cones with parameter $\chi = \epsilon = \pm 1$, which for graphene determines the sign of k_x, while for a Weyl metal giving an overall sign difference. The important difference between the two Hamiltonians is that in the Weyl Hamiltonian the 3D momentum is coupled to the Pauli matrices instead of the 2D momentum. In a Weyl semimetal we have energies

$$E = \pm v_F \sqrt{(k_x - \epsilon b_x)^2 + (k_y - \epsilon b_y)^2 + (k_z - \epsilon b_z)^2} + \epsilon b_0. \tag{1.4}$$

Therefore a perturbation in the z-direction simply shifts the k_z momentum, which only changes the location of the Weyl nodes. The Weyl nodes are not destroyed, as was the case for the Dirac points in graphene. This is why we say that the existence and stability of the Weyl nodes is guaranteed by the third dimension.

In the next Chapter, we will show that the Weyl nodes have topological properties, which is the reason Weyl metals are topological materials. The topological properties of these materials lead to remarkable consequences such as surface states with open Fermi surfaces, called Fermi arcs, and the chiral magnetic effect, which are all not present in graphene. This has caused a great interest in this field by condensed matter physicists. In this Thesis, we focus on the properties of the surface states in Weyl semimetals under the influence of a magnetic field. First, we introduce some key properties of Weyl metals further.

1.1 Topological properties

In 2005 Kane and Mele [4] discovered a new class of materials called topological insulators. These materials are insulators in the bulk, but allow for conducting surface states which are protected from local perturbations by topological properties of their band structure. While in the bulk the dispersion is gapped, the surfaces of topological insulators in 3D have a gapless Dirac dispersion like graphene. These surface states are protected by time-reversal symmetry. Since the surface has a gapless dispersion, conduction on the surface is possible. This remarkable discovery has led to an explosion of interest in topology in the condensed matter field. This led people to look into other topological materials, such as Weyl metals. Weyl metals are particularily interesting because they have topologically protected conducting surface states which are also chiral, which means the conducting electrons only move in one direction. The Dirac semimetal is degenerate in momentum space, which means two Weyl cones are lying on top of eachother. In this Thesis we consider a time-reversal symmetry broken Weyl semimetal. The symmetry is broken by the splitting vector $\mathbf{b} = (0, 0, b_z)$, pictured in Figure 1.2.

The topological nature of the Weyl nodes lies in the fact that they act, depending on the chirality, as a source or sink of Berry flux. In 1984, Michael Berry found that adiabatically transporting a system around a loop C by varying parameters R in its Hamiltonian $H(R)$, the system acquires a geometrical phase factor $e^{i\gamma(C)}$ called the Berry phase [5]. The Berry phase over a closed loop C in parameter space (momentum space in our case) is given by

$$\gamma = i \oint_C \mathrm{d}\mathbf{k} \, \langle u(\mathbf{k}) \,|\, \nabla_{\mathbf{k}} \,|\, u(\mathbf{k}) \rangle = \oint_C \mathrm{d}\mathbf{k} \cdot \mathbf{A}(\mathbf{k}), \tag{1.5}$$

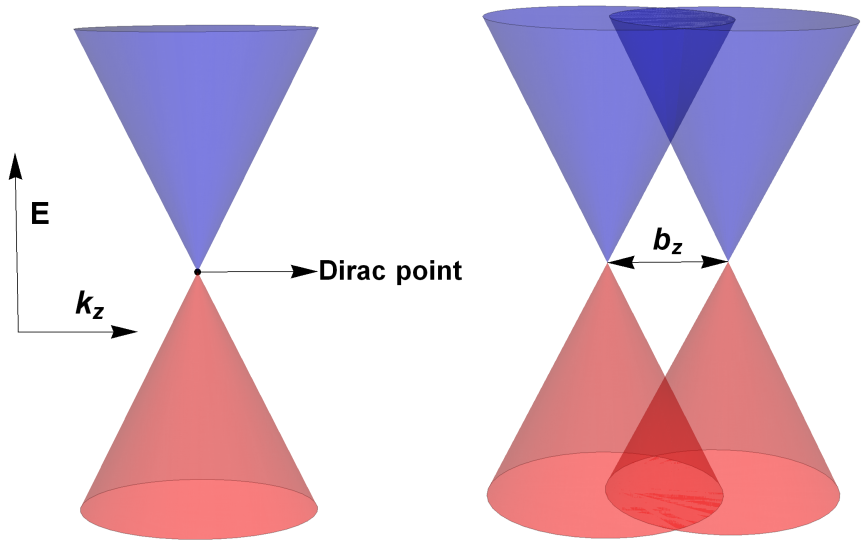

Figure 1.2 – Graphical representation of a single Dirac cone (left) and two Weyl cones (right), separated in momentum space by the splitting vector b_z.

where $u(\mathbf{k})$ are Bloch wave functions. We defined the Berry connection as $\mathbf{A}(\mathbf{k}) = i\,\langle u(\mathbf{k})\,|\,\nabla_{\mathbf{k}}\,|\,u(\mathbf{k})\rangle$. The Berry curvature is obtained by taking the rotation with respect to parameter space

$$\Omega(\mathbf{k}) = \nabla_{\mathbf{k}} \times \mathbf{A}(\mathbf{k}).$$

Using Stokes' theorem we can rewrite the Berry phase in terms of a surface integral over the Berry curvature, giving

$$\gamma = \int_S d\mathbf{S} \cdot \Omega(\mathbf{k}). \tag{1.6}$$

By the Chern-Gauss-Bonnet theorem, this integral is an integer multiple of 2π. The Chern number over a surface S in momentum space is defined by

$$C_S = \frac{1}{2\pi} \int_S d\mathbf{S} \cdot \Omega(\mathbf{k}). \tag{1.7}$$

If we take a surface enclosing the entire Brillouin zone of the semimetal and calculate the Chern number we get 0 (topologically trivial), since by periodicity in all directions, this is equivalent to a point. Therefore, the Chern number of all Weyl nodes together must vanish. However, if we take a surface in momentum space enclosing one of the Weyl nodes, the Chern number will be non-zero (topologically non-trivial). Taking the Hamiltonian 1.3, we can calculate the eigenstates and use them to find the Berry curvature of one node. We find

$$\Omega(\mathbf{k}) = -\epsilon \frac{\mathbf{k}}{2k^3}, \tag{1.8}$$

where $k = |\mathbf{k}|$, giving

$$C_S = \frac{1}{2\pi} \int_S d\mathbf{S} \cdot \Omega(\mathbf{k}) = \epsilon. \tag{1.9}$$

So enclosing a positive chirality node gives a Chern number of $+1$, while a negative chirality node gives -1. Consequently, the Weyl nodes must always come in pairs (sink, source) to result in a vanishing net Chern number. Using the Berry curvature 1.8, we find

$$\nabla_{\mathbf{k}} \cdot \Omega(\mathbf{k}) = \epsilon\delta(\mathbf{k}), \tag{1.10}$$

which shows that Weyl nodes are monopoles of Berry curvature. Since the topology has to be preserved, the Weyl nodes can only be destroyed by annihilating two nodes with opposite chirality, reverting back to a Dirac semimetal.

1.2 Surface states

A well known property of topological insulators is that they have topologically protected surface states. These states also appear on the surfaces of Weyl semimetals, but they have different properties. The Fermi surfaces of surface states are usually closed surfaces, but for Weyl semimetals they are open. The Berry flux coming from the Weyl nodes flows from the positive chirality cone to the negative chirality cone. So if we take a surface between the Weyl nodes, we get a non-zero Chern number. If we move this surface slightly left or right (but still between the nodes), we still have a non-zero Chern number. Therefore, we can generate a line of points between the Weyl nodes that have non-zero Chern number. By the bulk-boundary correspondence [6], for every point on this line the bulk is a topological insulator, and thus has a surface state. The Fermi surface of the surface state is an open line, which we call the Fermi arc. For instance, if we split the Weyl nodes up in the z-direction by $b_z > 0$, the Fermi arc exists for $|k_z| < b_z$. We will investigate the surface states and their behaviour under the influence of a magnetic field in Chapter 4.

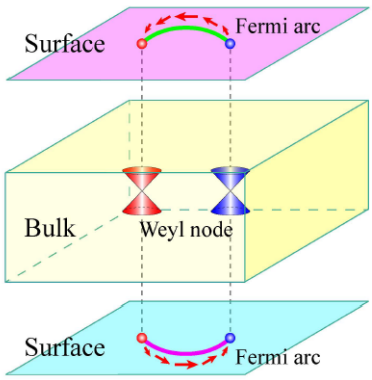

Figure 1.3 – Schematic picture of the Fermi arcs drawn on two surfaces, connected through the Weyl nodes in the bulk. Image taken from Ref. [7].

1.3 Chiral magnetic effect

The Chiral magnetic effect (CME) is one of the most interesting and exciting properties of Weyl semimetals. Charged particles in a magnetic field have quantized energy levels, called Landau levels. The energy separation of the Landau

levels depends on the strength of the magnetic field. However, thermal fluctuations broaden the energy levels into bands. Consequently, for low magnetic fields and high temperatures, the energy separation is too small to see the quantization, since the energy bands will overlap. That means we need strong enough magnetic fields to be able to see the Landau levels, which we assume to be the case throughout this Thesis. The lowest Landau level of a cone is chiral, which means that the particles in this state can only move in one direction. When we combine the magnetic field with an electric field, the so-called chiral anomaly appears. The action of massless Dirac fermions in (3+1) dimensions can have a chiral symmetry defined by $\psi \to e^{i\gamma^5\theta}\psi$, where ψ is a Dirac-spinor. By Noether's theorem, this symmetry has a corresponding conserved current $\partial_\mu J_5^\mu = 0$. Therefore we expect the number of chiral fermions to be conserved, so $\partial_t N_\pm = 0$. However, if we couple this equation to an external gauge field, we get an anomalous quantum correction which causes J_5 to not be conserved anymore:

$$\partial_\mu J_5^\mu = \frac{e^2}{2\pi^2\hbar^2}\mathbf{E}\cdot\mathbf{B}. \tag{1.11}$$

Since this current is no longer conserved, we get a chiral population imbalance, as $\partial_t(N_+ - N_-) \neq 0$ (see Figure 1.4). This is called the chiral anomaly.

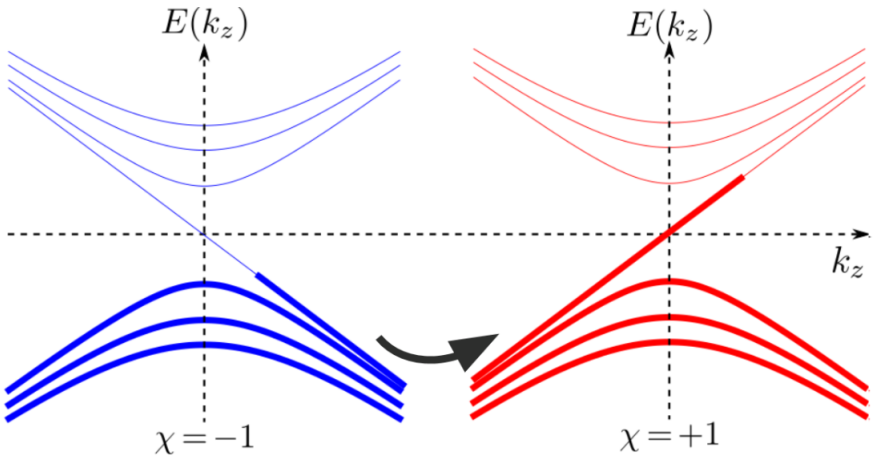

Figure 1.4 – The Landau level energies plotted as a function of the momentum k_z. The chirality in this picture is denoted by χ. After switching on the electric field, the momentum of the electrons is increased. This creates a chiral imbalance, causing a current to flow. In this picture the magnetic and electric fields are in the z-direction. Image made by Erik van der Wurff.

We can understand this result intuitively by taking a close look at the band structure. Switching on the electric field $\mathbf{E}$ creates a force $F = -e\mathbf{E}$ on the electrons. Since we have $\hbar\partial_t\mathbf{k} = e\mathbf{E}$, the momentum of the electrons is increased. Since the ground state is chiral, the electrons in the "$-$" chirality band will lose energy while the electrons in the "+" chirality band increase their energy (see Figure 1.4). The model we use has two seperate bands with different chirality. In a realistic band structure however, the two bands are connected, so a current will flow from one band to the other. Since the energies depend on the momentum in the direction of the magnetic field, the current flows in the direction of the magnetic field. This is called the chiral magnetic effect. The generated chiral

magnetic current is given by

$$\mathbf{J} = \frac{\mu_5 e^2}{2\pi^2}\mathbf{B}, \tag{1.12}$$

where μ_5 is the chiral chemical potential. Furthermore, the chiral magnetic current is dissipationless. This is a direct consequence of time-reversal symmetry. One could also look at it from another perspective. In general, a loss of energy is obtained by an electron scattering off something like an impurity. However, this assumes that there are quantum states available for the scattering process. Since the lowest Landau level is chiral, the only allowed states occupying this level are the ones that have the direction aligned with the chiral direction. Since scattering states by definition have different direction than the original direction, they are not available to the electrons.

1.4 Anomalous Hall effect

Next to the CME, there is another effect present in Weyl semimetals that makes these materials very interesting. In 1879 Edwin H. Hall made the important discovery that when a conductor is placed in a magnetic field perpendicular to the current, a voltage difference across the conductor appears, perpendicular to the magnetic field. The voltage difference appears because the charge carriers experience a Lorentz force, causing the charges to accumulate on one side of the conductor. This effect provided a tool to measure carrier concentration, which later proved to be very useful in developing the field of solid-state physics. Shortly after his discovery, Hall discovered that the effect he measured was much stronger in ferromagnetic conductors. This became known as the anomalous Hall effect (AHE). It was only after about a century that theoreticians figured out what caused this increased Hall current. The breakthrough for understanding the AHE was the formulation of the Berry phase, which we have shown is also very important in Weyl semimetals.

The anomalous Hall effect has two contributions: the intrinsic (related to the Berry phase) AHE and the extrinsic (impurity scattering) AHE. In a Weyl semimetal, it was shown that the extrinsic part is absent [8]. The current due to the AHE is

$$\mathbf{J} = \frac{e^2}{2\pi^2}\mathbf{b} \times \mathbf{E} \tag{1.13}$$

where $\mathbf{b}$ is the splitting vector and $\mathbf{E}$ the electric field. The reason that the AHE is particularily interesting in Weyl semimetal, is that the current is fully determined by the relative location of the Weyl nodes. The AHE relies directly on splitting the Weyl cones in momentum space by $\mathbf{b}$. Since the Weyl nodes are topologically protected and can only be removed by annihilating two opposite chirality nodes, the AHE current is also topologically protected in Weyl semimetals. This makes it very interesting to use Weyl semimetals for experiments with the AHE.

1.5 Experimental realizations

The first experimental discovery of a Weyl semimetal was made in 2015 in Tantalum Arsenide (TaAs) [9, 10, 11]. The theoretical work predicting the low energy

Weyl behaviour was already done half a year before [12]. Using photoemission spectroscopy (ARPES), the Fermi arcs were immediately observed as a key experimental signature. The experimentalists continued, using a technique called soft X-ray ARPES to gain insight into the bulk dispersion of the material. There they found experimental signatures of Weyl fermions, like Weyl cones and Weyl nodes. A very convincing result of the team's ARPES measurements is shown in Figure 1.5. This work opened the field for the experimental study of Weyl semimetals. Very shortly after, Weyl semimetals were discovered in Niobium Arsenide (NbAs) [13] and Tanalum Phosphide (TaP) [14]. Weyl cones have also been observed in photonic crystals [15].

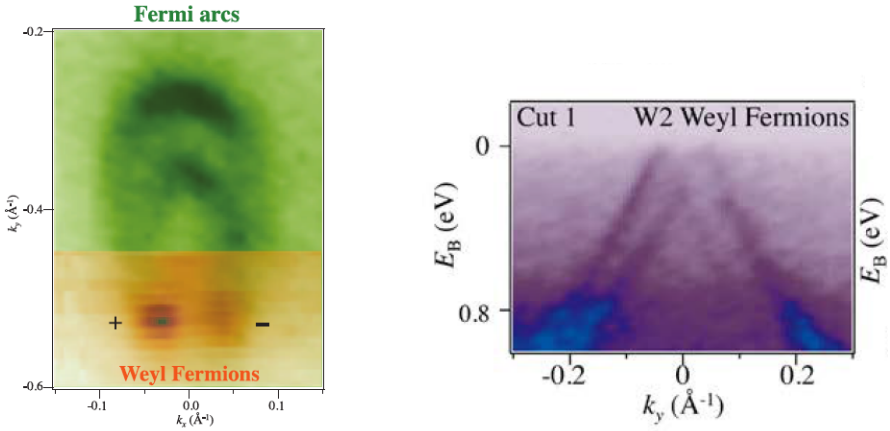

Figure 1.5 – ARPES maps of TaAs showing the Fermi arcs (left) and the Weyl cones (right). The Fermi arcs are indicated by the darker color. The chirality of the Weyl nodes are indicated by the plus and minus signs. The Fermi arcs correctly end at the Weyl nodes. Picture from Ref. [9].

Weyl semimetals are interesting for technological purposes, as the massless nature of the Weyl fermions could be used to conduct electric charge much faster through a material than normal electrons - a very important property for electronic circuits. Furthermore, Weyl semimetals also have dissipationless CME currents, another promising property for the future of electronic circuits. Graphene shares some of these properties, however 2D materials are not very practical for use in technology. Another advantage over graphene is the topological protection of the Weyl fermions, a feature which could be very useful in quantum computers. The experimental work we discussed above was done for so-called type-I Weyl semimetals. A recent topic of interest are type-II Weyl semimetals. These materials have tilted Dirac cones, such that the Fermi surface is no longer a point. These properties have been found for example in MoTe2 [16], WP2 and MoP2 [17]. These last two materials have also been shown to exhibit extremely high magnetoresistance [17].

1.6 Anomalous magnetic moment in Weyl semimetals

Another interesting feature of Weyl semimetals we will consider in this Thesis, is its large anomalous magnetic moment. When considering the Zeeman interaction of an electron's spin with an external magnetic field in vacuum, historically, the dimensionless magnetic moment $g_m = 2$ was derived by Dirac. However it

turned out to be a coincidence that this value is so close to 2. In 1947 a deviation from $g_m = 2$ was measured [18]. Shortly after, the Nobel-prize winning American physicist Julian Schwinger used quantum field theory to calculate this deviation of the magnetic moment of the electron due to the coupling with the photon [19]. This deviation is called the anomalous magnetic moment, defined by $a = \frac{g-2}{2}$. Schwinger found $a \approx 0.0011614$, which is close to the current best experimental value $a = 0.00115965218073$ [20].

Schwinger considered massive electrons in vacuum, however in Weyl semimetals electrons behave as massless particles around the band-touching points. This presents a problem, since the anomalous magnetic moment for massless electrons contains an infrared divergence [1]. However, if the photons couple to a finite density of electrons, photons acquire an effective mass at long wavelengths. This generates a screened Coulomb potential between the electrons, giving an infrared cutoff, which makes the anomalous magnetic moment finite. For typical parameters, the photon mass is found to be about three orders of magnitude smaller than the free electron mass. This implies that the Coulomb interaction has a relatively large range, which shows that the vertex corrections, pictured in Figure 1.6, can be of significant size.

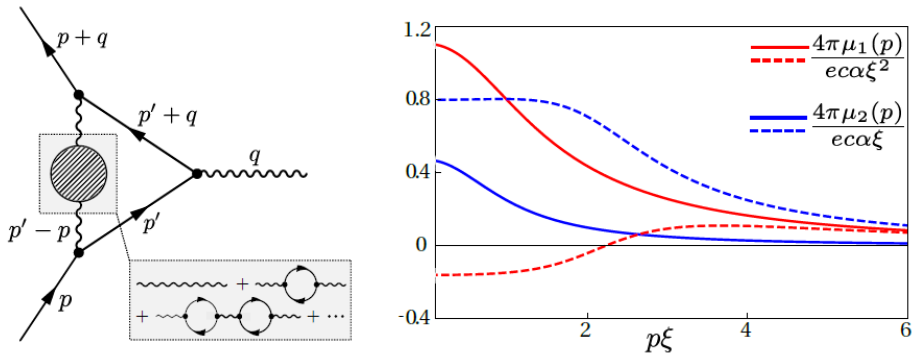

Figure 1.6 – Feynman diagram of the vertex correction to the magnetic moment (left). The wiggly lines denote photons while the fermions are denoted by straight lines. The dimensionless magnetic moments (right) for $k_F\xi = 1/4$ (solid lines) and $k_F\xi = 2$ (dashed lines), where ξ is the screening length $\xi = \sqrt{\pi/2g\bar{\alpha}k_F^2}$ with the dimensionless effective fine-structure constant $\bar{\alpha} \equiv e^2/4\pi\epsilon_0\hbar v_F$ and g the number of Weyl nodes. Pictures taken from Ref. [1].

In Ref. [1], the contribution from the anomalous magnetic moment was calculated to be

$$H_{\text{anomalous}} = -\left[\mu_1 \vec{p} \times \vec{\sigma}\right] \cdot \frac{\vec{E}}{v_F} - \left[\mu_2 \vec{\sigma} - \epsilon \mu_1 \vec{p}\right] \cdot \vec{B}, \tag{1.14}$$

where μ_1 and μ_2 are magnetic moments. These magnetic moments depend on the momentum, but become constant for large wavelengths. Throughout this Thesis, we use μ_1 and μ_2 as constants, which are their long-wavelength limit values. The first term is interpreted as a Rashba-spin-orbit coupling, while the second and third term are Zeeman-like terms. Note that the third term is dependent on the chirality of the cone and has the effect of tilting the cones. For typical parameter values, the authors of Ref. [1] find $\mu_1 k_F/\mu_B \approx 0.25$ and $\mu_2/\mu_B \approx 0.85$ where μ_B is the Bohr magneton. Hence, the anomalous effects are substantial, and could

measurably influence the semimetal.

One of the main motivations for writing this Thesis was the appearance of this large anomalous magnetic moment. In Ref. [1], it was found that for a constant external electric field, the Rashba spin-orbit term that follows from the anomalous magnetic moment vastly influences the surface states in certain cases. By looking at the surface states in a constant magnetic field, we can find the effect of the other anomalous terms, which couple to the magnetic field. Since the surface states were greatly influenced by the Rashba spin-orbit term, the surface states may also be significantly affected by the Zeeman terms. We will further expand on the effects of these anomalous terms in Chapter 3 and 4.

1.7 Outline

Now that we introduced some key features of Weyl metals, we will warm up by deriving the Landau level eigenstates and energies in the bulk of the metal in Chapter 2. We look at the Landau levels that appear for magnetic fields parallel and perpendicular to the band splitting b_z. The results that follow form the foundation for the following Chapters. We continue in Chapter 3 by focusing on the surface states in a half-infinite Weyl semimetal. For three separate cases, we derive the surface state wavefunction in the semimetal and the vacuum, and match the full wavefunction at the surface. First, we look at the surface state for zero magnetic field. Second, we use a WKB approximation to find the surface state for a magnetic field parallel to the surface. Third, we use the results of Chapter 2 to attempt to find the surface state for a magnetic field perpendicular to the surface. We find no solutions in this case, which leads us to conclude that there are no surface states in a half-infinite semimetal in a perpendicular magnetic field. At the end of Chapter 3, using the surface-state solutions we found for a magnetic field parallel to the surface, we look at the effects of the anomalous magnetic moment on the surface states. We continue in Chapter 4 by investigating surface states in a finite slab of Weyl semimetal. We find that solutions are possible, but very hard to find for low magnetic fields. Surprisingly, we find that closed magnetic orbits are possible in a finite Weyl semimetal. Particles in these orbits move over the surface between Weyl nodes, and continue to propagate through the bulk to the other surface. In the high magnetic field limit, we only have to consider the lowest Landau level, as the higher levels are separated in energy proportional to the square root of the field strength. We find analytical solutions of propagating states in the bulk, moving from surface to surface, with discrete energy levels. Next, we investigate how the energies of these states change when we add anomalous terms. We round off Chapter 4 by looking at the first order correction in the magnetic field to the lowest Landau level limit. The first order correction is found by adding one Landau level above the lowest level, and using numerics to investigate the effect on the energy levels. Finally, in Chapter 5, we summarize our results and discuss open questions.

Chapter 2

Landau Levels in the bulk

Charged particles in a magnetic field will move in orbits perpendicular to the magnetic field, due to the Lorentz force. The energy of these so-called cyclotron orbits quantize in a magnetic field, called Landau quantization. This is only observed if the magnetic field is high enough such that the separation of the energy levels is higher than the mean thermal energy : $\hbar\omega_c \gg k_B T$ where $\omega_c = qb/m$ is the cyclotron frequency. We assume this to be the case throughout this Thesis. In this Chapter we derive the energy levels of massless spin-1/2 Weyl fermions in a 3D Weyl semimetal, under influence of an external magnetic field. We work in units where $\hbar, v_F \equiv 1$ for simplicity and reintroduce SI units when it is relevant. A Weyl fermion obeys the Weyl equation, given by

$$\sigma^\mu \partial_\mu \psi = 0, \tag{2.1}$$

where $\sigma^\mu = (\sigma^0, \sigma^1, \sigma^2, \sigma^3)$ are Pauli matrices with $\sigma^0 = \mathbf{1}_{2\times 2}$ and ψ is a Weyl spinor. Two Weyl fermions of opposite chirality are described by the Dirac Hamiltonian

$$H = \gamma^0 \boldsymbol{\gamma} \cdot (-i\boldsymbol{\nabla}), \tag{2.2}$$

where we use the convention for the Dirac matrices

$$\gamma^0 = \begin{pmatrix} 0 & \mathbf{1}_2 \\ -\mathbf{1}_2 & 0 \end{pmatrix}, \gamma^i = \begin{pmatrix} 0 & \sigma_i \\ \sigma_i & 0 \end{pmatrix}.$$

To include the magnetic field we use the minimal substitution $-i\boldsymbol{\nabla} \to -i\boldsymbol{\nabla} + e\mathbf{A}$. Additionaly, to get a Weyl semimetal instead of a Dirac semimetal we break time-reversal symmetry by splitting the two bands up in momentum space by the band splitting vector $\mathbf{b}$, so we subtitute $\mathbf{k} \to \mathbf{k} - \epsilon\mathbf{b}$. Lastly, we assume no interactions between cones, so we will be able to describe the system as two separate two-by-two problems. Altogether this gives us the general Hamiltonian for a Weyl semimetal under influence of a magnetic field

$$H = \gamma^0 \left[\vec{\gamma} \cdot \left(-i\vec{\nabla} + e\vec{A} + \gamma^5 \vec{b} \right) \right], \tag{2.3}$$

where

$$\gamma^5 = \begin{pmatrix} -\mathbf{1}_2 & 0 \\ 0 & \mathbf{1}_2 \end{pmatrix}.$$

The Landau level eigenstates per cone are two-component Weyl spinors, which we write down in four components using the Dirac matrices. Throughout this

Thesis we assume the bands are split in the z-direction in momentum space, so $\mathbf{b} = (0, 0, b_z)$. We treat two cases, one where the magnetic field is parallel to the band splitting and the other where it is perpendicular. Splitting up the bands in other directions in momentum space can also be done, but offers no new insights.

2.1 Magnetic field parallel to band splitting

We start with the general Hamiltonian of a Weyl semimetal in a magnetic field, given by

$$H = \gamma^0 \left[\boldsymbol{\gamma} \cdot \left(-i\boldsymbol{\nabla} + e\mathbf{A} + \gamma^5 \mathbf{b} \right) \right]. \tag{2.4}$$

For $\mathbf{A} = b_0 = 0$, the spectrum is given by Eq. 1.4. Since we do not have interactions between cones, we have no off-diagonal elements. That means we can write the semimetal Hamiltonian 2.4 per cone in 2D using the chirality $\epsilon = \pm 1$,

$$H = \epsilon \left[(-i\boldsymbol{\nabla} + e\mathbf{A}) \cdot \boldsymbol{\sigma} - \epsilon b_z \sigma_3 \right]. \tag{2.5}$$

We take the magnetic field in the z-direction. To preserve translational invariance in the y,z directions, we choose the Landau gauge $\mathbf{A} = B(0, x, 0)$. We can assume plane waves in the y, z-direction, giving the ansatz $\psi(\mathbf{x}) = e^{ik_y y + ik_z z}\phi(x)$. We obtain a two-by-two problem per cone, with an effective Hamiltonian acting on a two-component spinor $\phi(x)$ that we can write as

$$H = \epsilon \begin{pmatrix} k_z - \epsilon b_z & -i\partial_x - i(eBx - k_y) \\ -i\partial_x + i(eBx - k_y) & -k_z + \epsilon b_z \end{pmatrix}.$$

Looking at the effective Hamiltonian, we see that the splitting of the Weyl nodes b_z simply shifts the momentum with direction depending on the chirality. We define the harmonic oscillator operators as

$$\begin{aligned} a^\dagger &= \frac{1}{\sqrt{2eB}}(p_x + i(eBx - k_y)), \\ a &= \frac{1}{\sqrt{2eB}}(p_x - i(eBx - k_y)), \end{aligned} \tag{2.6}$$

with $p_x = -i\partial_x$, which satisfy $[a, a^\dagger] = 1$. Note that there is a degeneracy in k_y hidden in the way we define the operators. This degeneracy is in the localization of the harmonic oscillator wave functions coming along with these operators (see Appendix A). We can write H using Eq. 2.6 as

$$H = \epsilon \begin{pmatrix} k_z - \epsilon b_z & -\sqrt{2eB}a^\dagger \\ -\sqrt{2eB}a & -k_z + \epsilon b_z) \end{pmatrix}. \tag{2.7}$$

The eigenstates are two-component spinors we denote by $\phi = \left(|\phi^+\rangle, |\phi^-\rangle \right)^T$. The Schrödinger equation $H\phi = E\phi$ gives a set of two equations

$$-\epsilon\sqrt{2eB}a^\dagger |\phi^-\rangle + \epsilon(k_z - \epsilon b_z) |\phi^+\rangle = E |\phi^+\rangle, \tag{2.8}$$

$$-\epsilon\sqrt{2eB}a |\phi^+\rangle - \epsilon(k_z - \epsilon b_z) |\phi^-\rangle = E |\phi^-\rangle, \tag{2.9}$$

where E is the energy of the system. Solving the second equation for $|\phi^-\rangle$ gives

$$|\phi^-\rangle = \frac{-\epsilon\sqrt{2eB}a}{E + \epsilon(k_z - \epsilon b_z)} |\phi^+\rangle, \tag{2.10}$$

which we can put into the first equation and solve for E, resulting in

$$E^2 \left|\phi^+\right\rangle = \left(2eBa^\dagger a + (k_z - \epsilon b_z)^2\right) \left|\phi^+\right\rangle . \tag{2.11}$$

The only operator acting on $|\phi^+\rangle$ is the number operator, so the solutions are harmonic oscillator states. We assume $|\phi^+\rangle = c\,|n\rangle$ with c some constant and put this back into 2.11, giving the energy levels (for $n > 0$)

$$E = \sqrt{2eBn + (k_z - \epsilon b_z)^2}. \tag{2.12}$$

The negative n give negative energies $E = -\sqrt{2eBn + (k_z - \epsilon b_z)^2}$, as we have particle-hole symmetry. Inserting $|\phi^+\rangle = c\,|n\rangle$ into the equation for $|\phi^-\rangle$ gives

$$\left|\phi^-\right\rangle = c\frac{-\epsilon\sqrt{2eBn}}{E + \epsilon(k_z - \epsilon b_z)} \left|n-1\right\rangle .$$

Note that $|\phi^-\rangle = 0$ for $n = 0$, so we have to treat this case seperately. Now that we know the eigenstates, we can use the normalization condition $\phi^T\phi = 1$ to find c, giving

$$c = \left(1 + \frac{2eBn}{\epsilon E + (k_z - \epsilon b_z)^2}\right)^{-1/2} . \tag{2.13}$$

To conclude, we get the eigenstates (for $|n| > 0$)

$$\phi_{n,\epsilon} = \begin{pmatrix} a_{n,\epsilon}\left|n\right\rangle \\ b_{n,\epsilon}\left|n-1\right\rangle \end{pmatrix},$$

with

$$\begin{aligned} a_{n,\epsilon} &= \left(1 + \frac{2eB|n|}{\epsilon E + (k_z - \epsilon b_z)^2}\right)^{-1/2} \\ b_{n,\epsilon} &= \frac{-\sqrt{2eB|n|}}{\epsilon E + (k_z - \epsilon b_z)} a_{n,\epsilon}. \end{aligned} \tag{2.14}$$

Note that for the negative energy states ($n < 0$) the energy switches sign. For $n = 0$, we get the normalized eigenstate

$$\phi_{0,\epsilon} = \begin{pmatrix} \left|0\right\rangle \\ 0 \end{pmatrix},$$

with its energy given by

$$H\phi_{0,\epsilon} = E_0\phi_{0,\epsilon} = \epsilon(k_z - \epsilon b_z)\phi_{0,\epsilon}.$$

We see that per cone there is only one sign for the ground state energy, determined by the chirality. Together with the dependence on k_z, this means the electrons only move in one direction. We call this the chiral ground state. The energy of the states above the ground state do not depend on the chirality. However, as we will see in Chapter 3, interaction effects from the anomalous magnetic moment can cause energy differences between cones, which will affect the surface states. The chiral ground state will turn out to be of profound importance when we look at surface states in Weyl semimetals.

Writing the eigenstates down in four components gives for $|n| > 0$

$$|\psi_n\rangle = C_{n,1} \begin{pmatrix} a_{n,1}|n\rangle \\ b_{n,1}|n-1\rangle \\ 0 \\ 0 \end{pmatrix} + C_{n,2} \begin{pmatrix} 0 \\ 0 \\ a_{n,-1}|n\rangle \\ b_{n,-1}|n-1\rangle \end{pmatrix},$$

with $E_n = \pm\sqrt{2eBn + (k_z - \epsilon b_z)^2}$ and $C_{n,1}, C_{n,2}$ constants. The energies for the two cones are plotted in Figure 2.1. The states above are linear combinations of states residing in one cone, as we do not have interactions between cones. These states are called the Landau level eigenstates.

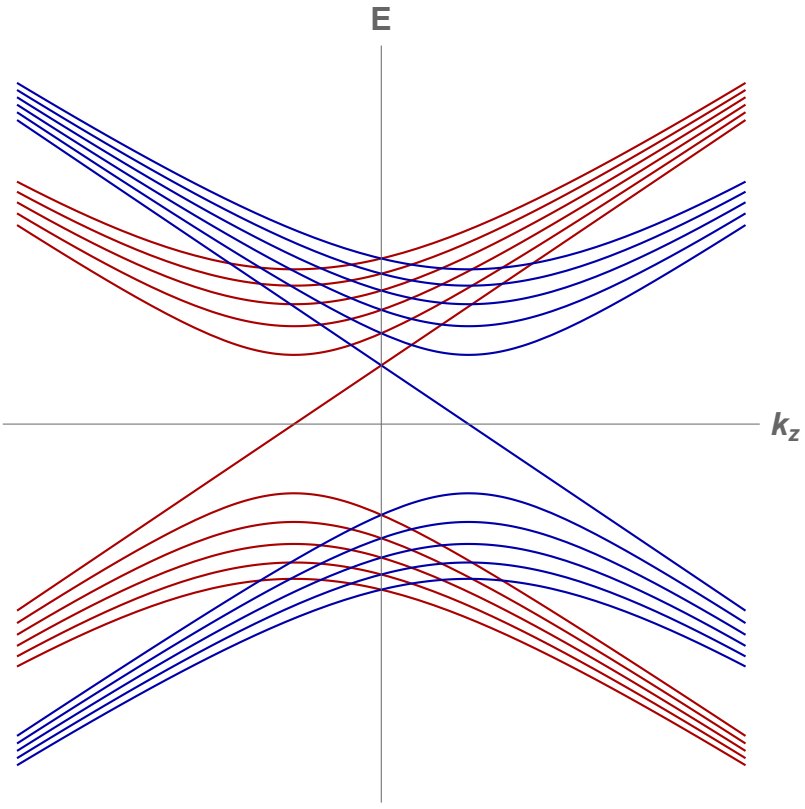

Figure 2.1 – Energies of the Landau levels of the $\epsilon = -1$ (red) and $\epsilon = 1$ (blue) Weyl cones as a function of k_z for $b_z \neq 0$.

2.2 Magnetic field perpendicular to band splitting

Now that we found the Landau levels in the bulk for $\mathbf{B} = B\hat{z}$, we look at a perpendicular magnetic field $\mathbf{B} = -B\hat{x}$. We include the magnetic field in the negative x-direction by minimal coupling and try to find the solutions in the bulk. The semimetal Hamiltonian per cone in 2D is given by

$$H = \epsilon\left[(-i\boldsymbol{\nabla} + e\mathbf{A}) \cdot \boldsymbol{\sigma} - \epsilon b_z \sigma_3\right]. \tag{2.15}$$

We choose the gauge $\mathbf{A} = (0, Bz, 0)$, breaking translational invariance in the z-direction. We have translational invariance in x and y, so we expect plane waves

in these directions. This gives us the ansatz $\psi(\mathbf{x}) = e^{ik_x x + ip_y y}\phi(z)$, leaving us with a one-dimensional problem in z. Using this ansatz, we get the Hamiltonian

$$\begin{aligned} H &= \epsilon\left[k_x\sigma_1 + (k_y + eBz)\sigma_2 - i\partial_z\sigma_3 - \epsilon b_z\sigma_3\right], \\ &= \epsilon\begin{pmatrix} -i\partial_z - \epsilon b_z & -i(k_y + eBz) + k_x \\ i(k_y + eBz) + k_x & i\partial_z + \epsilon b_z \end{pmatrix}. \end{aligned}$$

In the case of the magnetic field in the z-direction, we could immediately identify the ladder operators of the harmonic oscillator in the Hamiltonian. This time the parts which form the ladder operators, ∂_z and $i(k_y + eBz)$, are in different matrix elements. To resolve this issue, we apply a unitary transformation in spin space using the unitary matrix

$$V = \frac{1}{\sqrt{2}}\begin{pmatrix} 1 & 1 \\ 1 & -1 \end{pmatrix}. \tag{2.16}$$

Note that this will affect the eigenstates as well. The unitary transformation gives the rotated Hamiltonian $\tilde{H}$

$$\tilde{H} = V^\dagger H V = \epsilon\begin{pmatrix} k_x & -i\partial_z + i(eBz + k_y) - \epsilon b_z \\ -i\partial_z - i(eBz + k_y) - \epsilon b_z & -k_x \end{pmatrix}. \tag{2.17}$$

We define the operators

$$\begin{aligned} a^\dagger &= \frac{1}{\sqrt{2eB}}(-i\partial_z + i(eBz + k_y) - \epsilon b_z) \\ a &= \frac{1}{\sqrt{2eB}}(-i\partial_z - i(eBz + k_y) - \epsilon b_z), \end{aligned} \tag{2.18}$$

satisfying $[a, a^\dagger] = 1$ and rewrite Hamiltonian 2.17 in the now familiar form

$$\tilde{H} = \epsilon\begin{pmatrix} k_x & \sqrt{2eB}a^\dagger \\ \sqrt{2eB}a & -k_x \end{pmatrix}. \tag{2.19}$$

The addition of the $-\epsilon b_z$ term in the operators will add a phase $e^{\epsilon i b_z z}$ to the harmonic oscillator wavefunctions (see Appendix A). This approach turns out to be much easier than the approach taken in Ref. [21], where perturbation theory is attempted. The energy should ultimately not depend on b_z, so there is probably a mistake in this calculation. A first-order perturbation calculation on the wave function confirms that a band splitting perpendicular to the magnetic field generates a phase on the harmonic oscillator states (Appendix B). Since the Hamiltonian is of the same form as the Hamiltonian for the magnetic field in the z-direction 2.7, we can immediately conclude that the energies are given by (for $n > 0$)

$$E_n = \pm\sqrt{2eBn + k_x^2}, \tag{2.20}$$

similar to 2.12. We can also copy the eigenstates, giving the new coefficients

$$\begin{aligned} a_{n,\epsilon} &= \left(1 + \frac{2eBn}{(E + \epsilon k_x)^2}\right)^{-1/2}, \\ b_{n,\epsilon} &= \frac{\sqrt{2eBn}}{\epsilon E + k_x}a_n. \end{aligned} \tag{2.21}$$

Writing this down again in four components, we have the mutually orthogonal set of eigenstates for $|n| > 0$

$$|\psi_n\rangle = C_{n,1} \begin{pmatrix} a_{n,1} e^{ib_z z} |n\rangle \\ b_{n,1} e^{ib_z z} |n-1\rangle \\ 0 \\ 0 \end{pmatrix} + C_{n,2} \begin{pmatrix} 0 \\ 0 \\ a_{n,-1} e^{-ib_z z} |n\rangle \\ b_{n,-1} e^{-ib_z z} |n-1\rangle \end{pmatrix},$$

where we explicitly added the phase to the original harmonic oscillator wave functions denoted by $|n\rangle$. Note that this are harmonic oscillator states in the z-direction, while in the previous section we had harmonic oscillator states in the x-direction. The ground states are given by

$$|\psi_{0,\epsilon=1}\rangle = \begin{pmatrix} e^{ib_z z} |0\rangle \\ 0 \\ 0 \\ 0 \end{pmatrix} \quad |\psi_{0,\epsilon=-1}\rangle = \begin{pmatrix} 0 \\ 0 \\ e^{-ib_z z} |0\rangle \\ 0 \end{pmatrix}.$$

As before, the chiral ground state energy turns out to have no ambiguity in sign and is given by $E_0 = \epsilon k_x$. The energies of the Landau levels are depicted in Figure 2.2.

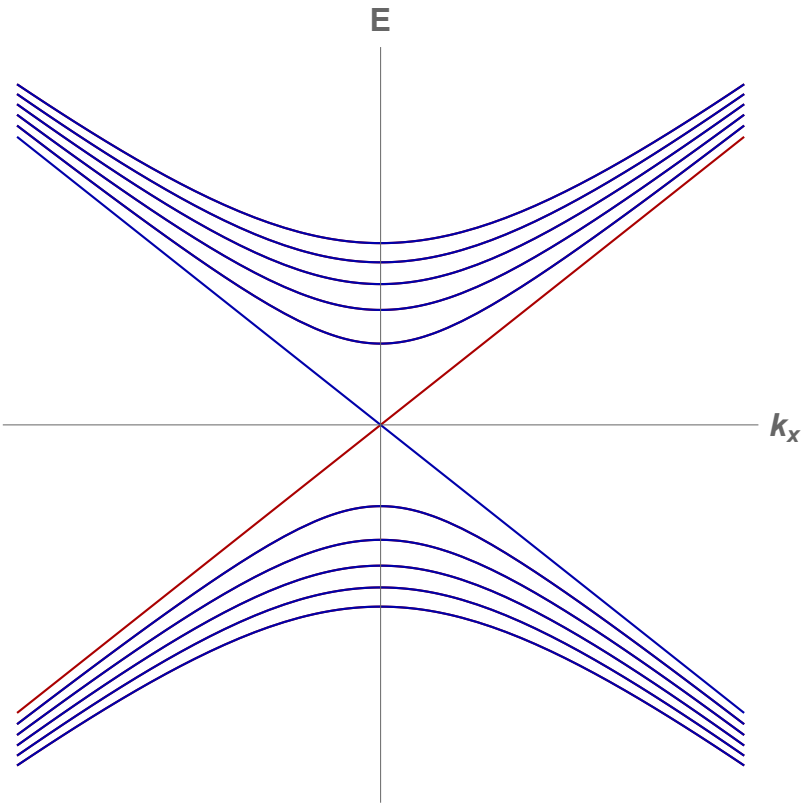

Figure 2.2 – Energies of the Landau levels of the $\epsilon = -1$ (red) and $\epsilon = 1$ (blue) Weyl cones as a function of k_x. The energies are no longer shifted by b_z, so the Landau levels above the zeroth level lie on top of each other.

We can put the eigenstates back in the original spin basis using the V-matrix

given in Eq. 2.16. In two-component notation, we get

$$|\psi_n^v\rangle = V\,|\psi_n\rangle = \frac{1}{\sqrt{2}}\left(1+\frac{2eBn}{(\epsilon E+k_x)^2}\right)^{-1/2}\begin{pmatrix}|n\rangle + \frac{\sqrt{2eBn}}{\epsilon E+k_x}\,|n-1\rangle\\ |n\rangle - \frac{\sqrt{2eBn}}{\epsilon E+k_x}\,|n-1\rangle\end{pmatrix},$$
$$|\psi_0^v\rangle = V\,|\psi_0\rangle = \begin{pmatrix}e^{\epsilon i b_z z}\,|0\rangle\\ e^{\epsilon i b_z z}\,|0\rangle\end{pmatrix}.$$

The chiral ground state is spin-polarized in the x-direction, which is in the direction of the magnetic field, as we have

$$\langle\psi_0^v\,|\,\sigma_1\,|\,\psi_0^v\rangle = 1,$$
$$\langle\psi_0^v\,|\,\sigma_2\,|\,\psi_0^v\rangle = 0,$$
$$\langle\psi_0^v\,|\,\sigma_3\,|\,\psi_0^v\rangle = 0.$$

This will turn out to have interesting consequences. For $n > 0$ the states are no longer spin-polarized, as we get

$$\langle\psi_n^v\,|\,\sigma_1\,|\,\psi_n^v\rangle = \frac{-2eBn+(\epsilon E+k_x)^2}{2eBn+(\epsilon E+k_x)^2},$$
$$\langle\psi_n^v\,|\,\sigma_2\,|\,\psi_n^v\rangle = 0,$$
$$\langle\psi_n^v\,|\,\sigma_3\,|\,\psi_n^v\rangle = 0.$$

We have now found the energy levels and eigenstates of a Weyl semimetal in a magnetic field. We split the Weyl cones up in momentum space in the z-direction and showed that in a parallel magnetic field, this shifts the momentum k_z. In a perpendicular magnetic field, this adds a phase to the harmonic oscillator wavefunctions in the Landau level eigenstates. Furthermore, we showed that the lowest Landau level is chiral and spin-polarized. These results will be the foundation of the next Chapters. In Chapter 3, we will investigate surface states in a half-infinite semimetal. To find the surface state wavefunction in the bulk, we slightly modify the results we found in this Chapter.

Chapter 3

Surface States in a half-infinite Weyl semimetal

One of the remarkable properties of Weyl semimetals is the existence of conducting surface states. These states decay exponentially away from the surface, and are topologically protected. As we will show, the surface states are gapless and chiral. These states are experimentally observable by measuring their Fermi arcs, serving as a key experimental signature for Weyl semimetals.

We start out by investigating surface states absent a magnetic field, and continue by looking at the influence of a magnetic field on the surface states. In our model we look at a half-infinite semimetal bordering a vacuum of mass m at $x = 0$. The setup is pictured in Figure 3.1. The mass m is artificial but serves as a barrier for electrons to leave the bulk. We assume the metal is infinitely long in the y, z and positive x directions such that we can disregard boundary effects in those directions. We break time reversal symmetry by splitting up the Weyl cones in the z direction in momentum space by $b_z > 0$.

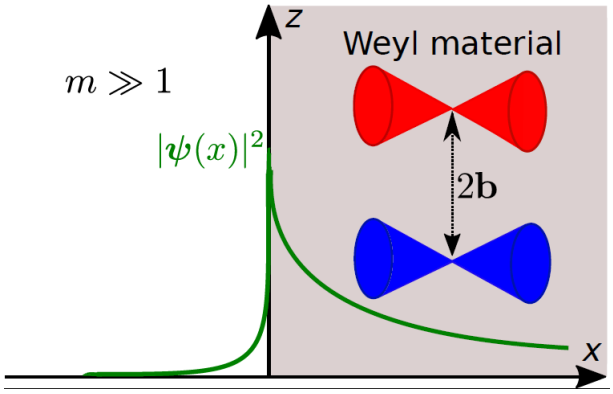

Figure 3.1 – Schematic picture of our model for a Weyl semimetal. The model consists of a vacuum for $x < 0$ and a Weyl semimetal for $x > 0$ with time reversal symmetry breaking vector $\mathbf{b}$. The green line denotes the amplitude of a surface state, which is decaying away from the surface. Picture taken from Ref. [1].

3.1 Zero magnetic field

The case of zero magnetic field is already treated in Ref. [21]. We briefly repeat the main calculations and results. The Hamiltonian describing the system is

$$H = \gamma^0 \left[\boldsymbol{\gamma} \cdot \left(-i\nabla + \theta(x)\gamma^5 b_z \hat{z} \right) + \theta(-x) i m \right], \tag{3.1}$$

where $\theta(x)$ is the Heaviside step function and we add the imaginary unit to the mass to make that term Hermitian, since $(\gamma^0)^\dagger = -\gamma^0$ in our case. We will solve the problem in the semimetal and vacuum sides seperately and match the solutions on the boundary $x = 0$.

3.1.1 Semimetal

In the semimetal, we have the Hamiltonian

$$H = \gamma^0 \left[\boldsymbol{\gamma} \cdot \left(-i\nabla + \gamma^5 b_z \hat{z} \right) \right]. \tag{3.2}$$

Since we have translational symmetry in y, z, we assume plane waves in these directions. We want to find surface states, so we assume that the wavefunction decays exponentially away from the surface. Additionaly, as we have no interactions between cones, we know the wavefunction to consist of a linear combination of the eigenstates of the single cones. This gives us the ansatz

$$|\psi(\mathbf{x})\rangle = e^{ik_y y + ik_z z} \left(C_1 e^{-\lambda_1 x} |\psi_{\epsilon=1}\rangle + C_2 e^{-\lambda_{-1} x} |\psi_{\epsilon=-1}\rangle \right), \tag{3.3}$$

where $Re[\lambda_\pm] > 0$ since we want exponential decay for $x > 0$, and $|\psi_\epsilon\rangle$ are 4-component vectors in the cone with chirality ϵ. Since the Hamiltonian has no off-diagonal elements, we can rewrite the Schrödinger equation $H\psi(\mathbf{x}) = E\psi(\mathbf{x})$ per cone as

$$\partial_x |\psi(\mathbf{x})\rangle = Q |\psi(\mathbf{x})\rangle = \lambda_\pm |\psi(\mathbf{x})\rangle \tag{3.4}$$

where Q is defined by

$$Q = -i\gamma^1 \left[\gamma^0 E - \gamma^2 k_y - \gamma^3 \left(k_z + \gamma^5 b_z \right) \right]. \tag{3.5}$$

Eq. 3.4 is easily solved for $\lambda_\pm$, giving

$$\lambda_\epsilon = \sqrt{-E^2 + k_y^2 + (k_z - \epsilon b_z)^2}. \tag{3.6}$$

The corresponding eigenvectors are given by

$$|\psi_{\epsilon=1}\rangle = c_1 \begin{pmatrix} \frac{i\left(-k_y + \sqrt{k_y^2 + (k_z - b_z)^2 - E^2}\right)}{-E - k_z + b_z} \\ 1 \\ 0 \\ 0 \end{pmatrix}, \quad |\psi_{\epsilon=-1}\rangle = c_{-1} \begin{pmatrix} 0 \\ 0 \\ \frac{i\left(k_y - \sqrt{k_y^2 + (k_z + b_z)^2 - E^2}\right)}{-E + k_z + b_z} \\ 1 \end{pmatrix}, \tag{3.7}$$

where $c_{\pm 1}$ are normalization constants. So the surface state wave function in the semimetal is given by

$$|\psi(\mathbf{x})\rangle = e^{ik_y y + ik_z z} \left(C_1 e^{-\lambda_1 x} |\psi_{\epsilon=1}\rangle + C_2 e^{-\lambda_{-1} x} |\psi_{\epsilon=-1}\rangle \right), \tag{3.8}$$

where C_1, C_2, E are to be determined by matching the wave functions in the vacuum and the semimetal at the boundary. We proceed using the same method to find the wave function in the vacuum.

3.1.2 Vacuum

In the vacuum, we have the Hamiltonian

$$H = \gamma^0 \left[\boldsymbol{\gamma} \cdot (-i\nabla) + im\right]. \tag{3.9}$$

We use the exponentially decaying ansatz $\psi(x) = e^{-\lambda x}\phi(x)$, where $\phi(x)$ is a spinor, and with negative λ as we want it to decay for negative x. However, this time we have off-diagonal elements in the Hamiltonian. Consequently, we will not be able to write the eigenstates using only two components. We get the ansatz

$$|\tilde{\psi}(\mathbf{x})\rangle = e^{ik_y y + ik_z z}\tilde{C}_i e^{\tilde{\lambda}_i x} |\tilde{\psi}\rangle_i \,, \tag{3.10}$$

where $|\tilde{\psi}\rangle_i$ are four-component spinors. Again rewriting the Schrödinger equation, we get a similar equation to Eq. 3.4, with

$$Q = -i\gamma^1 \left[\gamma^0 E - \gamma^2 k_y - \gamma_3 k_z - im\right]. \tag{3.11}$$

We find only one negative solution

$$\tilde{\lambda} = -\sqrt{-E^2 + k_y^2 + k_z^2 + m^2}.$$

Thus, the eigenstates $|\tilde{\psi}\rangle_i$ are given by

$$|\tilde{\psi}_1\rangle = \frac{\tilde{c}_1}{m}\begin{pmatrix} -k_y + \tilde{\lambda} \\ i(E + k_z) \\ 0 \\ m \end{pmatrix}, \quad |\tilde{\psi}_2\rangle = \frac{\tilde{c}_2}{m}\begin{pmatrix} i(E - k_z) \\ -k_y - \tilde{\lambda} \\ m \\ 0 \end{pmatrix}, \tag{3.12}$$

where $\tilde{c_{1,2}}$ are normalization constants. So the solution in the Dirac vacuum is given by

$$|\tilde{\psi}(\mathbf{x})\rangle = e^{\sqrt{-E^2 + k_y^2 + k_z^2 + m^2}x}\left(\tilde{C}_1 |\tilde{\psi}_1\rangle + \tilde{C}_2 |\tilde{\psi}_2\rangle\right), \tag{3.13}$$

where $\tilde{C}_1, \tilde{C}_2, E$ have to be determined in the matching procedure.

3.1.3 Matching at the boundary

By continuity, we demand that the two wave functions have to be matched at the boundary: $|\tilde{\psi}(x = 0)\rangle = |\psi(x = 0)\rangle$. We also demand that the wave function is normalized:

$$\int_{-\infty}^{0} dx \, \langle\tilde{\psi}(x)|\tilde{\psi}(x)\rangle + \int_{0}^{\infty} dx \, \langle\psi(x) \,|\, \psi(x)\rangle = 1. \tag{3.14}$$

Together these two conditions give five equations, and we have five unknowns: the four coefficients $\tilde{C}_1, \tilde{C}_2, C_1, C_2$ and the energy E. The matching equations define a matrix problem

$$M(\tilde{C}_1, \tilde{C}_2, C_1, C_2)^T = 0,$$

which has non-trivial solutions when $\det(M) = 0$. This condition gives us the allowed energies for the surface states. We find the gapless solution

$$E = -k_y, \tag{3.15}$$

which only holds for $|k_z| < b_z$. This solution shows that the surface state is chiral, so the electrons on the surface can only move in one direction, the y-direction.

Using this solution, together with the normalization condition 3.14, we can find the full wave function. We take the limit $m \to \infty$, disallowing the electrons from leaving the semimetal, to simplify the expressions. This forces the vacuum wavefunction to only exist on the surface $x = 0$. We find the wavefunctions to be

$$|\tilde{\psi}(x=0)\rangle = ce^{ik_y y + ik_z z} \begin{pmatrix} 1 \\ -1 \\ 1 \\ 1 \end{pmatrix} \tag{3.16}$$

$$|\psi(\mathbf{x})\rangle = ce^{ik_y y + ik_z z} \left(e^{-(b_z+k_z)x} \begin{pmatrix} i \\ -1 \\ 0 \\ 0 \end{pmatrix} + e^{-(b_z-k_z)x} \begin{pmatrix} 0 \\ 0 \\ i \\ 1 \end{pmatrix} \right). \tag{3.17}$$

We see that the wave functions decay slightly differently for each cone away from the surface. After taking the $m \to \infty$ limit, the wave function is zero in the vacuum, but nonzero on the surface. This shows that we could not have simply taken the boundary condition to be that $|\psi(x=0)\rangle = 0$, as this could not have given the same result. The important difference is that the wave function still has spin structure on the boundary which we cannot ignore. Note that for $|k_z| = b_z$, the wavefunction actually does not decay in the bulk. This will turn out to be very important later on.

3.1.4 Anomalous effects with zero magnetic field

In the zero magnetic field case, we can still have anomalous effects due to an external electric field $\mathbf{E}$. These anomalous effects were derived in [1]. The first term in Hamiltonian 1.14 represents the anomalous Rashba spin-orbit coupling, originating from the Coulomb interaction between electrons. Adding this term to the Hamiltonian gives the anomalous Hamiltonian

$$H = \gamma^0 \boldsymbol{\gamma} \cdot \left[-i\nabla - \gamma^5 b_z \hat{z} + (\mu_1 \mathbf{E} \times b_z \hat{z}) - i\gamma^5 (\mu_1 \mathbf{E} \times \nabla) \right]. \tag{3.18}$$

Since k_y and k_z are still good quantum numbers, we can still use the same ansatz $|\psi(\mathbf{x})\rangle = e^{ik_y y + ik_z z}\phi(x)$, giving a one-dimensional problem in x. Since we use a half-infinite slab of Weyl semimetal, assume exponential decay in the negative x-direction, giving $\phi(x) \propto e^{-\lambda x}$, with $\lambda < 0$. As before, we want to find the effective matrix Q and determine its eigenvalues. There are three different situations. An electric field in the y-direction does not affect the surface state dispersion and Fermi arc. An electric field in the z-direction $\mathbf{E} = E_z \hat{z}$ (not to be mistaken with the energy E) does affect the dispersion. Following Ref. [21], we find, similar to Eq. 3.4,

$$Q = \frac{1}{1+E_z^2} \begin{pmatrix} \boldsymbol{\sigma} \cdot \mathbf{v}_+^z & 0 \\ 0 & \boldsymbol{\sigma} \cdot \mathbf{v}_-^z \end{pmatrix}, \tag{3.19}$$

where $\mathbf{v}_\pm^z = \big((\mp iE \mp E_z(k_z \pm b_z), iE_z E - (k_z \pm b_z), k_y(1+E_z^2)\big)$. The negative eigenvalue of this matrix is

$$\lambda^z = -\sqrt{\frac{(k_z \pm b_z)^2 + k_y^2(1+E_z)^2 - E^2}{1+E_z^2}}, \tag{3.20}$$

which we put into the wave function for the semimetal. The new wave function is matched at $x = 0$ with the unchanged vacuum wave function, giving the dispersion

$$E = -k_y\sqrt{1+E_z^2}, \tag{3.21}$$

which still has the Fermi arc $|k_z| < b_z$. In SI units, we get the dispersion

$$E = -v_F k_y\sqrt{1+E_z^2}. \tag{3.22}$$

So the electric field in this case increases the Fermi velocity by a factor $\sqrt{1+E_z^2}$, but does not alter the linearity in k_y of the dispersion nor the Fermi arc.

The most interesting case is when we take the electric field perpendicular to the surface, $\mathbf{E} = E_x\hat{x}$. This gives the effective matrix

$$Q = \begin{pmatrix} \boldsymbol{\sigma}\cdot\mathbf{v}_+^x & 0 \\ 0 & \boldsymbol{\sigma}\cdot\mathbf{v}_-^x \end{pmatrix}, \tag{3.23}$$

where $\mathbf{v}_\pm^x = (\mp iE, E_x k_y \mp (k_z \pm b_z), k_y \pm E_x(k_z \pm b_z))$. The effective matrix has positive eigenvalues

$$\lambda_\pm^x = \sqrt{(k_z \pm b_z)^2(1+E_x^2) + k_y^2(1+E_x^2) - E^2}. \tag{3.24}$$

The matching procedure gives the dispersion

$$E = -\frac{(1-E_x)^2 b_z k_y + E_x(k_y^2 + k_z^2 - b_z^2)}{\sqrt{(b_z + E_x k_y)^2 + E_x^2 k_z^2}}, \tag{3.25}$$

which is no longer linear in k_y, and is no longer defined on a straight Fermi arc. Instead, the solution is now only defined in the exterior of the two circles defined by

$$\left(k_y + \frac{b_z}{E_x}\right)^2 + \left(k_z \pm \frac{b_z}{2}(1 + \frac{1}{E_x^2})\right)^2 = \frac{b_z^2}{4}\left(1+\frac{1}{E_x}\right)^2.$$

Inside these two circles, there are no surface states and the problem corresponds to a topologically trivial insulator. A density plot of the dispersion and the new Fermi arc is depicted in Figure 3.2.

3.2 Magnetic field parallel to surface

In this section we consider a magnetic field parallel to the band splitting b_z and the surface, so $\mathbf{B} = B\hat{z}$. We can choose our gauge such that A has a component in the x-direction, for example $\mathbf{A} = B(-y, 0, 0)$ or in the y-direction $\mathbf{A} = B(0, x, 0)$. In the first case we break translation symmetry in the y-direction, which causes k_y to no longer be a good quantum number. That means the result $E = -k_y$ we obtained in the zero magnetic field case, is no longer valid. In the second case, minimal substitution gives $k_y \to k_y + eBx$. But since the boundary is at $x = 0$, this term in first instance does not contribute to the surface state dispersion. While the surface state dispersion is unaffected, the decaying wave function may still be modified. Since we add a term eBx to the Hamiltonian, we can no longer

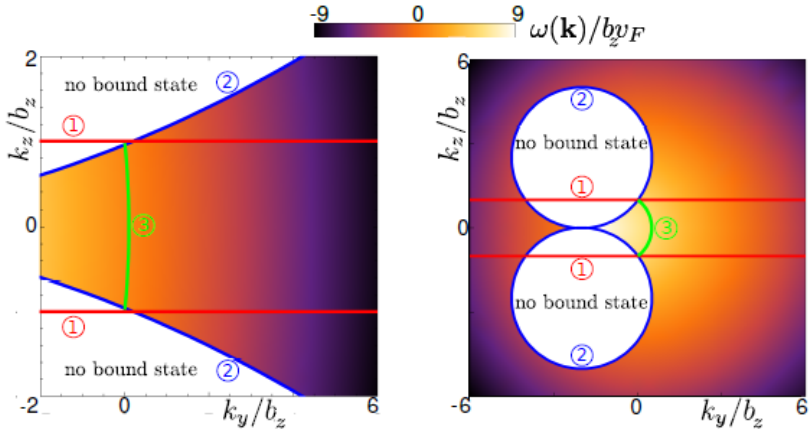

Figure 3.2 – Density plots of the dimensionless dispersion $\omega(\mathbf{k})/b_z v_F$ as a function of the dimensionless momenta k_z/b_z, k_y/b_z for $\bar{E}_x = \mu_1 E_x/\hbar v_F^2 = 1/10$ (left) and $\bar{E}_x = 1/2$ (right). The red lines ① indicate the allowed region for surface states for zero electric field (see previous section). The blue lines ② indicate the new allowed region for surface states, including the electric field. The green lines ③ indicate the Fermi arc, which is no longer a straight line. The white regions indicate regions where no surface state is supported. Picture adapted from Ref. [1].

use the exponential ansatz $\psi(x) = e^{-\lambda x}$. The solutions are found using a WKB approximation in Ref. [21]. In the vacuum the wave function becomes

$$|\tilde{\psi}(\mathbf{x})\rangle = c e^{ik_y y + ik_z z} e^{-\tilde{\lambda}(x)} \begin{pmatrix} i \\ i \\ 1 \\ 1 \end{pmatrix}, \tag{3.26}$$

where c is a constant of normalization and

$$\tilde{\lambda}(x) = \int_0^x \mathrm{d}x' \sqrt{-k_y^2 + k_z^2 + (k_y + eBx')^2 + m^2}$$

Note that we could not have found this using an exponential ansatz. The wave function in the semimetal becomes

$$\begin{aligned} |\psi(x)\rangle =& c e^{ik_y y + ik_z z} \sqrt{\frac{\lambda_-(0)}{\lambda_-(x)}} \sqrt{\frac{k_y + eBx + \lambda_-(x)}{k_y + \lambda_-(0)}} e^{\lambda_1(x)} \begin{pmatrix} 0 \\ 0 \\ -i\frac{k_y + eBx - \lambda_-(x)}{E - k_z + b_z} \\ 1 \end{pmatrix} + \\ & c e^{ik_y y + ik_z z} \sqrt{\frac{\lambda_+(0)}{\lambda_+(x)}} \sqrt{\frac{k_y + eBx + \lambda_+(x)}{k_y + \lambda_+(0)}} e^{\lambda_2(x)} \begin{pmatrix} i\frac{k_y + eBx - \lambda_+(x)}{E + k_z + b_z} \\ 1 \\ 0 \\ 0 \end{pmatrix}, \end{aligned}$$

where

$$\begin{aligned} \lambda_1(x) &= \int_0^x \mathrm{d}x' \lambda_-(x'), \quad \lambda_2(x) = \int_0^x \mathrm{d}x' \lambda_+(x'), \\ \lambda_\pm(x) &= \sqrt{-k_y^2 + (k_y + eBx)^2 + (k_z \pm b_z)^2}. \end{aligned}$$

In the zero magnetic field case, we found that the wavefunctions for each cone decay differently, with all the x-dependence in the exponential. In this case, we see that all four components of the wave function do not fall off at the same rate, since the components have different dependencies on x. At the surface at $x = 0$, the same wave function as the zero magnetic field case is found, as expected.

3.3 Magnetic field perpendicular to the surface

In this section we consider a magnetic field in the negative x-direction, perpendicular to the band splitting b_z and the surface. A magnetic field in the z-direction generates cyclotron orbits in the xy plane, coinciding with the direction of the surface state dispersion in the zero magnetic field case. This intuitively justifies that the magnetic field does not influence the surface states in this case. Electrons propagating through the bulk in the x-direction are also pulled back by the Lorentz force. Therefore, we do not expect bound states to no longer be bounded when adding a magnetic field parallel to the surface. That is no longer the case for a magnetic field in the x-direction, since there is no Lorentz force on electrons propagating through the bulk in the x-direction. That means we expect vastly different results for the surface states than in the previous section.

3.3.1 Solutions in semimetal bulk

In the semimetal we have the Hamiltonian

$$H = \epsilon \left[(-i\boldsymbol{\nabla} + e\mathbf{A}) \cdot \boldsymbol{\sigma} - \epsilon b_z \sigma_3 \right], \tag{3.27}$$

with the gauge $\mathbf{A} = (0, Bz, 0)$. We want to find states that live on the surface and exponentially decay away from the surface. Using the Landau level solutions we found in Chapter 2, the most general ansatz we can make is a linear combination of the Landau levels combined with exponential decay away from the surface. A sensible ansatz is therefore

$$|\psi_{\mathrm{SM}}(\vec{x})\rangle = e^{ik_y y} \sum_{n \geq 0} \left(e^{-\lambda_n x} \left[C_{n,1} |\psi_{n,1}\rangle + C_{n,2} |\psi_{n,-1}\rangle \right] \right),$$

where $C_{n,1}, C_{n,2}$ are coefficients to be determined in the matching procedure.

We now look at how the Hamiltonian acts on the individual Landau level states $e^{ik_y y} e^{\lambda_n x} |\psi_n\rangle$. We rotate the Hamiltonian in spin space using the unitary transformation matrix V given in Eq. 2.16. This gives us the Hamiltonian

$$V^\dagger H V = \epsilon \begin{pmatrix} -i\lambda_n & -i\partial_z + i(eBz + k_y) - \epsilon b_z \\ -i\partial_z - i(eBz + k_y) - \epsilon b_z & i\lambda_n \end{pmatrix}$$

We recognize the form of the Hamiltonian of the Landau levels in the bulk 2.19 with $k_x = -i\lambda_n$. Therefore, we can immediately conclude that for $n > 0$, we get $E = \pm\sqrt{2eBn - \lambda_n^2}$. For $n = 0$ we get $E = -\epsilon i \lambda_0$, indicating that λ_0 is

imaginary. Using the results from Chapter 2, we get

$$|\psi_{0,1}\rangle = \begin{pmatrix} e^{ib_z z}|0\rangle \\ 0 \\ 0 \\ 0 \end{pmatrix} \quad |\psi_{0,-1}\rangle = \begin{pmatrix} 0 \\ 0 \\ e^{-ib_z z}|0\rangle \\ 0 \end{pmatrix},$$

$$|\psi_{n,1}\rangle = \begin{pmatrix} a_{n,1}\ e^{ib_z z}|n\rangle \\ b_{n,1}\ e^{ib_z z}|n-1\rangle \\ 0 \\ 0 \end{pmatrix} \quad |\psi_{n,-1}\rangle = \begin{pmatrix} 0 \\ 0 \\ a_{n,-1}\ e^{-ib_z z}|n\rangle \\ b_{n,-1}\ e^{-ib_z z}|n-1\rangle \end{pmatrix},$$

where a_n,b_n are given by Eq. 2.21 with $k_x = -i\lambda_n$. We can rewrite λ_n in terms of E, giving $\lambda_n = \pm\sqrt{2eBn - E^2}$ and $\lambda_0 = \epsilon i E$. We discard the negative λ_n since we want surface states which decay for increasing x. We also see that for a fixed energy there are certain Landau levels for which λ_n is real and others where there is no real solution. Therefore we want to fix some energy E and see if there are real solutions for λ_n. If these solutions exist, there are surface states. This also means that we can have a linear combination of these Landau levels with some higher Landau levels exponentially decaying away from the surface and some lower levels propagating through the semimetal.

We can transform the wave function back to the original spin basis using the V matrix again. This gives the wave function

$$|\psi_{\mathrm{SM}}(\vec{x})\rangle = e^{ik_y y}\left[C_{0,1}e^{iEx}e^{ib_z z}\begin{pmatrix}|0\rangle\\|0\rangle\\0\\0\end{pmatrix} + C_{0,2}e^{-iEx}e^{-ib_z z}\begin{pmatrix}0\\0\\|0\rangle\\|0\rangle\end{pmatrix}\right]$$
$$+ e^{ik_y y}\sum_{n>0}\left(\frac{e^{\lambda_n x}}{\sqrt{2}}\left[C_{n,1}|\psi^v_{n,1}\rangle + C_{n,2}|\psi^v_{n,-1}\rangle\right]\right),$$

with

$$|\psi^v_{n,1}\rangle = e^{ib_z z}\begin{pmatrix}\frac{i}{\sqrt{2}}|n\rangle + \frac{i\sqrt{2eBn}}{\sqrt{2}(E-i\lambda_n)}|n-1\rangle\\ \frac{i}{\sqrt{2}}|n\rangle - \frac{i\sqrt{2eBn}}{\sqrt{2}(E-i\lambda_n)}|n-1\rangle\\0\\0\end{pmatrix}$$

$$|\psi^v_{n,-1}\rangle = e^{-ib_z z}\begin{pmatrix}0\\0\\ \frac{i}{\sqrt{2}}|n\rangle + \frac{i\sqrt{2eBn}}{\sqrt{2}(-E-i\lambda_n)}|n-1\rangle\\ \frac{i}{\sqrt{2}}|n\rangle - \frac{i\sqrt{2eBn}}{\sqrt{2}(-E-i\lambda_n)}|n-1\rangle\end{pmatrix}.$$

We have now found the full solutions to the Landau level eigenstates in the bulk. We continue by calculating the expectation value of the spin of the Landau level states again. This gives

$$\langle\psi^v_n\,|\,\boldsymbol{\sigma}_i\,|\,\psi^v_n\rangle = 0,$$

where we use $\boldsymbol{\sigma}_i = \sigma_i \oplus \sigma_i$. Note that this is different from the bulk states, where we found non-zero expectation value for the spin in the x-direction. The ground

state is still the same,

$$|\psi_{0,\epsilon}\rangle = \begin{pmatrix} e^{i\epsilon b_z z}\,|0\rangle \\ 0 \end{pmatrix},$$

so we find that the ground state is still spin-polarized,

$$\begin{aligned}\langle\psi_0^v\,|\,\sigma_1\,|\,\psi_0^v\rangle &= 1,\\ \langle\psi_0^v\,|\,\sigma_2\,|\,\psi_0^v\rangle &= 0,\\ \langle\psi_0^v\,|\,\sigma_3\,|\,\psi_0^v\rangle &= 0.\end{aligned}$$

3.3.2 Solutions in vacuum

In the vacuum we have the Hamiltonian

$$H = \gamma^0\left[\vec{\gamma}\cdot(-i\nabla + e\vec{A}) + im\right]$$

We make the ansatz for the wavefunction in the vacuum

$$|\tilde{\psi}(\mathbf{x})\rangle = e^{ik_y y}\sum_n \tilde{c}_{n,m}e^{\tilde{\lambda}_m x}\,|\tilde{\psi}_n\rangle\,,$$

where $|\tilde{\psi}_n\rangle$ are the Landau-level states we found in the bulk, minus the phase from the splitting of the cones. We rotate the Hamiltonian in spin space using the unitary transformation matrix

$$V = \frac{i}{\sqrt{2}}\begin{pmatrix} 1 & 1 & 0 & 0\\ 1 & -1 & 0 & 0\\ 0 & 0 & 1 & 1\\ 0 & 0 & 1 & -1\end{pmatrix},$$

giving the Hamiltonian

$$\begin{aligned}V^\dagger H V &= \begin{pmatrix} -i\tilde{\lambda}_n & -i\partial_z + i(eBz+k_y) & im & 0\\ -i\partial_z - i(eBz+k_y) & i\tilde{\lambda}_n & 0 & im\\ -im & 0 & i\tilde{\lambda}_n & i\partial_z - i(eBz+k_y)\\ 0 & -im & i\partial_z + i(eBz+k_y) & i\lambda_n\end{pmatrix}\\ &= \begin{pmatrix} -i\tilde{\lambda}_n & \sqrt{2eBn}a^\dagger & im & 0\\ \sqrt{2eBn}a & i\tilde{\lambda}_n & 0 & im\\ -im & 0 & i\tilde{\lambda}_n & -\sqrt{2eBn}a^\dagger\\ 0 & -im & -\sqrt{2eBn}a & -i\tilde{\lambda}_n\end{pmatrix}.\end{aligned}$$

This Hamiltonian is slightly different from the Hamiltonian for the Landau levels due to the mass term. We can square the Hamiltonian to find the eigenenergies, giving

$$E_n = \pm\sqrt{2eBn + m^2 - \tilde{\lambda}_n^2}. \tag{3.28}$$

Additionaly, we can rewrite $\tilde{\lambda}_n$ in terms of E, giving

$$\tilde{\lambda}_n = \pm\sqrt{2eBn + m^2 - E^2}. \tag{3.29}$$

We discard the negative solution since it blows up for $x \to -\infty$. So the wavefunction is given by

$$|\tilde{\psi}(\mathbf{x})\rangle = e^{ik_y y}\sum_{n=0}^{\infty}\tilde{c}_n e^{-\tilde{\lambda}_n x}\,|\tilde{\psi}_n\rangle\,,$$

where $\tilde{\lambda}_n = -\sqrt{2eBn + m^2 - E^2}$. Since the mass now couples the Landau level states, the eigenstates have the form

$$|\tilde{\psi}_n\rangle = \begin{pmatrix} \tilde{a}_n |n\rangle \\ \tilde{b}_n |n-1\rangle \\ \tilde{a}'_n |n\rangle \\ \tilde{b}'_n |n-1\rangle \end{pmatrix}$$

for $n > 0$. The Schrödinger equation gives the 4 equations

$$\begin{aligned} -i\tilde{\lambda}_n \tilde{a}_n + \sqrt{2eBn}\tilde{b}_n + im\tilde{a}'_n &= E_n \tilde{a}_n, \\ \sqrt{2eBn}\tilde{a}_n + i\tilde{\lambda}_n \tilde{b}_n + im\tilde{b}'_n &= E_n \tilde{b}_n, \\ -im\tilde{a}_n + i\tilde{\lambda}_n \tilde{a}'_n - \sqrt{2eBn}\tilde{b}'_n &= E_n \tilde{a}'_n, \\ -im\tilde{b}_n - \sqrt{2eBn}\tilde{a}'_n - i\tilde{\lambda}_n \tilde{b}'_n &= E_n \tilde{b}'_n. \end{aligned}$$

Solving this system gives four solutions, given by

$$\begin{aligned} |\tilde{\psi}_{n,1}\rangle &= \frac{1}{\sqrt{2(2eBn + m^2)}} \begin{pmatrix} i\sqrt{2eBn}\,|n\rangle \\ (iE_n - \tilde{\lambda}_n)\,|n-1\rangle \\ 0 \\ m\,|n-1\rangle \end{pmatrix}, \\ |\tilde{\psi}_{n,2}\rangle &= \frac{1}{\sqrt{2(2eBn + m^2)}} \begin{pmatrix} (iE_n + \tilde{\lambda}_n)\,|n\rangle \\ i\sqrt{2eBn}\,|n-1\rangle \\ m\,|n\rangle \\ 0 \end{pmatrix}, \end{aligned} \tag{3.30}$$

where E_n, given by Eq. 4.2, can be positive and negative. We can change back to the original spin basis using the V matrix again. We get the states

$$\begin{aligned} |\tilde{\psi}^v_{n,1}\rangle = V\,|\tilde{\psi}_1\rangle &= \frac{1}{2\sqrt{2eBn + m^2}} \begin{pmatrix} i\sqrt{2eBn}\,|n\rangle + (iE - \tilde{\lambda}_n)\,|n-1\rangle \\ i\sqrt{2eBn}\,|n\rangle - (iE - \tilde{\lambda}_n)\,|n-1\rangle \\ m\,|n-1\rangle \\ -m\,|n-1\rangle \end{pmatrix}, \\ |\tilde{\psi}^v_{n,2}\rangle = V\,|\tilde{\psi}_2\rangle &= \frac{1}{2\sqrt{2eBn + m^2}} \begin{pmatrix} i\sqrt{2eBn}\,|n-1\rangle + (iE + \tilde{\lambda}_n)\,|n\rangle \\ (iE + \tilde{\lambda}_n)\,|n\rangle - i\sqrt{2eBn}\,|n-1\rangle \\ m\,|n\rangle \\ m\,|n\rangle \end{pmatrix}. \end{aligned}$$

Now that we are in the correct spin basis, we can compute the expectation value of the spin in the x-direction of the different solutions. This gives

$$\begin{aligned} \langle\tilde{\psi}^v_{n,1}|\boldsymbol{\sigma}_x|\tilde{\psi}^v_{n,1}\rangle &= -\frac{m^2}{2eBn + m^2}, \\ \langle\tilde{\psi}^v_{n,2}|\boldsymbol{\sigma}_x|\tilde{\psi}^v_{n,2}\rangle &= \frac{m^2}{2eBn + m^2}, \end{aligned}$$

which is the same for both signs of the energy. We see that the first two solutions ($|\tilde{\psi}^v_{n,1}\rangle$ with positive and negative energy) have spin directed in the negative x-direction which is in the direction of the magnetic field. The direction of the expectation value of the spin of the other two solutions are opposite to the field. In the $m \to \infty$ limit however, the spin is polarized in the positive and negative

x-direction. The lowest Landau level is spin-polarized for any m. The zeroth Landau level states have the form

$$|\tilde{\psi}_0\rangle = \begin{pmatrix} a_0\,|0\rangle \\ 0 \\ b_0\,|0\rangle \\ 0 \end{pmatrix}.$$

We get two solutions, a positive and a negative energy state given by

$$|\tilde{\psi}_0\rangle = \begin{pmatrix} \frac{im}{\sqrt{2}(E-i\tilde{\lambda}_0)}\,|0\rangle \\ 0 \\ \frac{1}{\sqrt{2}}\,|0\rangle \\ 0 \end{pmatrix},$$

where $E = \pm\sqrt{m^2 - \tilde{\lambda}_0^2}$ for the positive and negative energy state. We can transform the states back to the original spin basis, giving

$$|\tilde{\psi}_0^v\rangle = V\,|\tilde{\psi}_0\rangle = \frac{1}{\sqrt{2}} \begin{pmatrix} \frac{im}{\sqrt{2}(E-i\tilde{\lambda}_0)}\,|0\rangle \\ \frac{im}{\sqrt{2}(E-i\tilde{\lambda}_0)}\,|0\rangle \\ \frac{1}{\sqrt{2}}\,|0\rangle \\ \frac{1}{\sqrt{2}}\,|0\rangle \end{pmatrix}.$$

Now we can calculate the expectation value of the spin in the x-direction. This gives

$$\langle\tilde{\psi}_0^v|\boldsymbol{\sigma}_x|\psi_0^v\rangle = \frac{1}{2}\left(2|a_0^2| + 2|b_0|^2\right) = \frac{1}{2}\left(\frac{m^2}{E^2+\tilde{\lambda}_0^2} + 1\right) = 1$$

for both the positive and negative energy states. The expectation value of the spin in the other directions is zero, so the zeroth Landau level in the vacuum is also spin-polarized.

3.3.3 Matching

Now that we found the full wave functions in the vacuum and in the semimetal, we have to match them at the boundary $x = 0$. In the last two sections, we found the wave functions

$$|\psi_{SM}(\mathbf{x})\rangle = e^{ik_y y}e^{-\lambda_0 x}\left[C_{0,1}\begin{pmatrix} e^{ib_z z}|0\rangle \\ 0 \\ 0 \\ 0\end{pmatrix} + C_{0,2}\begin{pmatrix} 0 \\ 0 \\ e^{-ib_z z}|0\rangle \\ 0\end{pmatrix}\right] +$$

$$e^{ik_y y}\sum_{n>0}^{\infty} e^{-\lambda_n x}\left[C_{n,1}\begin{pmatrix} a_{n,1} & e^{ib_z z}|n\rangle \\ b_{n,1} & e^{ib_z z}|n-1\rangle \\ 0 & \\ 0 & \end{pmatrix} + C_{n,2}\begin{pmatrix} 0 & \\ 0 & \\ a_{n,-1} & e^{-ib_z z}|n\rangle \\ b_{n,-1} & e^{-ib_z z}|n-1\rangle\end{pmatrix}\right],$$

$$|\tilde{\psi}(\mathbf{x})\rangle = e^{ik_y y}e^{-\tilde{\lambda}_0 x}\tilde{C}_0\begin{pmatrix} \frac{im}{\sqrt{2}(E+i\tilde{\lambda}_0)}|0\rangle \\ 0 \\ \frac{1}{\sqrt{2}}|0\rangle \\ 0\end{pmatrix}$$

$$+ e^{ik_y y}\sum_{n=1}^{\infty}\frac{e^{-\tilde{\lambda}_n x}}{\sqrt{2(2eBn+m^2)}}\left[\tilde{C}_{n,1}\begin{pmatrix} i\sqrt{2eBn}\,|n\rangle \\ (iE-\tilde{\lambda}_n)\,|n-1\rangle \\ 0 \\ m\,|n-1\rangle\end{pmatrix} + \tilde{C}_{n,2}\begin{pmatrix} (iE+\tilde{\lambda}_n)\,|n\rangle \\ i\sqrt{2eBn}\,|n-1\rangle \\ m\,|n\rangle \\ 0\end{pmatrix}\right]$$

$$= e^{ik_y y}e^{-\tilde{\lambda}_0 x}\tilde{C}_0|\tilde{\psi}_0\rangle + e^{ik_y y}\sum_{n=1}^{\infty}e^{-\tilde{\lambda}_n x}\left[\tilde{C}_{n,1}|\tilde{\psi}_{n,1}\rangle + \tilde{C}_{n,2}|\tilde{\psi}_{n,2}\rangle\right],$$

where $\lambda_n = \sqrt{2eBn - E^2}$, $\tilde{\lambda}_n = -\sqrt{2eBn + m^2 - E^2}$. We want to match these wave functions at the boundary, so we set $|\psi_{SM}(x=0)\rangle = |\tilde{\psi}(x=0)\rangle$. We can now project with some vector containing harmonic oscillator states from the left. On the semimetal side we have a factor $e^{ib_z z}$, generating overlap with every harmonic oscillator state, given by the matrix elements $P_{n,m} \equiv \langle m|e^{\epsilon i b_z z}|n\rangle$. The states $|n\rangle$ are given by (see Appendix)

$$|n\rangle = \frac{i^n}{\sqrt{2^n n!}}\left(\frac{eB}{\pi}\right)^{1/4} e^{-\frac{(eBz+k_y)^2}{2eB}} H_n\left(\frac{1}{\sqrt{eB}}(eBz+k_y)\right), \tag{3.31}$$

where $H_n(x)$ are Hermite polynomials. For the diagonal elements, we get

$$P_{n,n} = \langle n|e^{\epsilon i b_z z}|n\rangle = \frac{1}{2^n n!}\left(\frac{eB}{\pi}\right)^{1/2}\int_{-\infty}^{\infty}dz\;\; e^{-\frac{2(eBz+k_y)^2}{2eB}}e^{\epsilon i b_z z}H_n^2\left(\frac{1}{\sqrt{eB}}(eBz+k_y)\right)$$

$$= \frac{1}{2^n n!}\left(\frac{eB}{\pi}\right)^{1/2} e^{-\frac{b_z^2}{4eB}-\frac{i\epsilon b_z k_y}{eB}}\int_{-\infty}^{\infty}dz\;\; e^{-\frac{(eBz+k_y-\frac{1}{2}i\epsilon b_z)^2}{eB}}H_n^2\left(\frac{1}{\sqrt{eB}}(eBz+k_y)\right),$$

where we completed the square in the exponential. We define $\eta = \frac{eBz+k_y-\frac{1}{2}i\epsilon b_z}{\sqrt{eB}}$ and rewrite the integral in terms of η, giving

$$P_{n,n} = \frac{1}{2^n n!}\left(\frac{eB}{\pi}\right)^{1/2} e^{-\frac{b_z^2}{4eB}-\frac{i\epsilon b_z k_y}{eB}}\int\frac{d\eta}{\sqrt{eB}}\;\; e^{-\eta^2}H_n^2\left(\eta+\frac{\epsilon i b_z}{2\sqrt{eB}}\right).$$

The integral we have now can be found in Gradshteyn [22]. The general form found there is

$$\int_{-\infty}^{\infty} dx e^{-x^2} H_m(x+y) H_n(x+z) = 2^n \pi^{1/2} m! y^{n-m} L_m^{n-m}(-2yz) \quad (m \leq n), \tag{3.32}$$

where L_n^{n-m} are generalized Laguerre polynomials. In this case, using 3.32, we have 'simple' Laguerre polynomials L_n^0, giving

$$\begin{aligned} P_{n,n} &= \frac{1}{2^n n!} \left(\frac{eB}{\pi}\right)^{1/2} e^{-\frac{b_z^2}{4eB} - \frac{i\epsilon b_z k_y}{eB}} \left[2^n \pi^{1/2} (n!) L_n^0 \left(-2(\frac{i\epsilon b_z}{2\sqrt{eB}})^2\right)\right] \\ &= e^{-\frac{b_z^2}{4eB} - \frac{i\epsilon b_z k_y}{eB}} L_n^0 \left(\frac{b_z^2}{2eB}\right). \end{aligned}$$

Similarily, the off-diagonal elements have generalized Laguerre polynomials L_n^α, giving

$$P_{m,n} = \frac{2^{\max(n,m)} \min(n,m)!}{\sqrt{2^{n+m} n! m!}} e^{-\frac{b_z^2}{4eB} - i\frac{\epsilon b_z k_y}{eB}} \left(\frac{i\epsilon b_z}{2\sqrt{eB}}\right)^{|n-m|} L_{\min(n,m)}^{|n-m|} \left(\frac{b_z^2}{2eB}\right). \tag{3.33}$$

Now that we have found these matrix elements, we can try to set up a system of equations by projecting with different states. On the semimetal side, we can project with two different vectors onto the lowest Landau level, $(\langle 0|, 0, 0, 0)$ and $(0, 0, \langle 0|, 0)$. The higher Landau levels have four different projections per level, giving us a total of two plus 4 equations per Landau level above the zeroth level. These are all the equations we are able to find, as other projections on the vacuum or semimetal side would simply yield zero. Finally, we have the normalization of the wavefunction, adding one equation. So altogether, if we take Landau levels into account up to the n-th level, we have $3 + 4n$ equations. If we look at the amount of coefficients, we see that there are two coefficients per level on the semimetal side, $C_{n,1}$ and $C_{n,2}$. On the vacuum side, we have one coefficient $\tilde{C}_0$ plus two coefficients, $\tilde{C}_{n,1}$ and $\tilde{C}_{n,2}$, per level above the zeroth level in the vacuum. Furthermore, we still have the energy E as an unknown. In total, we have $4+4n$ unknowns, which is one more than the amount of equations. That means we have an underdetermined system, so we cannot find a unique solution. Therefore, in the half-infinite semimetal, there are no surface state solutions. In Chapter 4, we will find surface state solutions in a finite slab of Weyl semimetal, and show why there are no solutions possible in the half-infinite semimetal. First, we stay in the half-infinite semimetal and look at the anomalous effects on the surface states in a magnetic field parallel to the surface.

3.4 Anomalous magnetic effects

Since we found no surface state solutions for a magnetic field perpendicular to the surface, in this section we only treat the magnetic field parallel to the surface, $\mathbf{B} = B\hat{z}$. We follow Ref. [21], where these results have been derived. Adding the anomalous terms relevant to the magnetic field from Hamiltonian 1.14, we get the Hamiltonian

$$H = \gamma^0 \boldsymbol{\gamma} \cdot \left[-i\nabla - \gamma^5 b_z \hat{z}\right] - \gamma^5 \left[\gamma^0 \gamma^3 \mu_2 + \mu_1 (k_z + \gamma^5 b_z)\right] B. \tag{3.34}$$

We treat the two new terms seperately. The first term scaling with μ_2, is an anomalous Zeeman term. Adding only this term gives the effective matrix

$$Q = -i\gamma^1 \left(\gamma^0 E - \gamma^2 \left[k_y + eBx\right] - \gamma^3 \left[k_z + \gamma^5 (b_z + \mu_2 B)\right]\right), \tag{3.35}$$

which is the effective matrix for zero magnetic field given in Eq. 3.5 with $b_z \to b_z + \mu_2 B$. So we conclude that we find the same surface state with energy $E = -k_y$ and with the anomalous effect extending the Fermi arc as $|k_z| < b_z + \mu_2 B$.

The second term, scaling with μ_1, is a term that tilts the Weyl cones. Adding this term to the Hamiltonian gives the effective matrix

$$Q = -i\gamma^1 \left(\gamma^0 \left[E - \gamma^5 \mu_1 (k_z - \gamma^5 b_z) B\right] - \gamma^2 \left[k_y + eBx\right] - \gamma^3 \left[k_z + \gamma^5 b_z\right]\right). \tag{3.36}$$

This is no longer simply a shift, but rather something more difficult. The resulting dispersion is vastly different from the dispersion in Eq. 3.15, which was found ignoring anomalous effects. It is given by

$$E = \mu_1 B b_z \left(1 - \frac{k_z^2}{b_z^2}\right) - k_y \sqrt{1 - (\mu_1 B)^2 \frac{k_z^2}{b_z^2}}, \tag{3.37}$$

which correctly reverts back to $E = -k_y$ for $\mu_1 = 0$. This is an interesting result, since the energy now depends on the splitting of the Weyl cones b_z. Ofcourse, $b_z = 0$ presents a problem, but in that case we have a Dirac semimetal, which does not have surface states at all. The allowed region in momentum space now depends on the magnetic field in a more complicated manner. The region is bounded by two hyperbolic curves defined by

$$k_y = \frac{k_z \pm b_z}{\mu_1 B k_z} \sqrt{b_z^2 - (\mu_1 B k_z)^2}. \tag{3.38}$$

The allowed region is drawn in Figure 3.3.

The two effects combined are given by the Hamiltonian 1.14, giving

$$Q = -i\gamma^1 \left(\gamma^0 \left[E - \gamma^5 \mu_1 (k_z - \gamma^5 b_z) B\right] - \gamma^2 \left[k_y + eBx\right] - \gamma^3 \left[k_z - \gamma^5 (b_z + \mu_2 B)\right]\right). \tag{3.39}$$

The surface state dispersion with both anomalous effects is then given by

$$E = \mu_1 B b_z \left(1 - \frac{k_z^2}{b_z (b_z + \mu_2 B)}\right) - k_y \sqrt{1 - (\mu_1 B)^2 \left(\frac{k_z}{b_z + \mu_2 B}\right)^2}. \tag{3.40}$$

Interestingly, the surface state dispersion now depends on the anomalous magnetic moment μ_2 because it Zeeman shifts b_z. Adding just the Zeeman term only influenced the allowed region in momentum space, because the energy did not depend on b_z. The allowed region changes only slightly, since we only shift $b_z \to b_z + \mu_2 B$, and is now given by the two hyperbolic curves

$$k_y = \frac{k_z \pm (b_z + \mu_2 B)}{\mu_1 B k_z} \sqrt{(b_z + \mu_2 B)^2 - (\mu_1 B k_z)^2}. \tag{3.41}$$

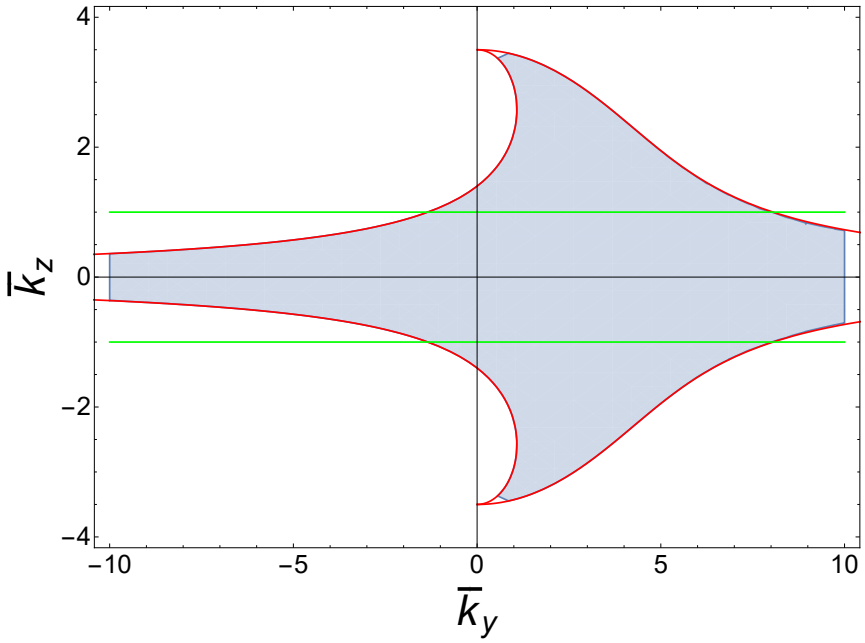

Figure 3.3 – The allowed region defined by Eq. 6.1 (red) for $\frac{\mu_1 B}{\hbar v_F} = 0.4$, compared to the non-anomalous region (green), for dimensionless $\bar{k}_{y,z} = k_{y,z}/b_z$. Picture taken from Ref. [21].

This concludes the anomalous effects on the surface states for a magnetic field parallel to the band splitting and surface. In this Chapter, we found surface states on a Weyl semimetal for zero and low magnetic fields. For zero magnetic field, we found a linear, chiral dispersion, only depending on k_y. Further on in the Chapter, we included anomalous effects, and found a non-linear dispersion which depends on k_z and b_z as well as k_y. For a magnetic field parallel to the surface, we found the same dispersion as for the zero magnetic field case. However, when including anomalous effects, we found that the anomalous magnetic effects significantly alter the dispersion, which now also depends on μ_1, μ_2, b_z and k_z. For a low magnetic field perpendicular to the surface, we were not able to find solutions for the surface state. However, in the next Chapter we will find solutions for surface states under influence of a strong perpendicular magnetic field. When we find the solutions, we can look at the anomalous effects on those surface states.

Chapter 4

Surface states on a finite slab of Weyl semimetal

In Chapter 3, we found no bound surface state solutions in a half-infinite Weyl semimetal in a magnetic field perpendicular to the surface. However, if we take a finite slab of Weyl semimetal by adding another surface on the right, we will find surface state solutions. The new model is pictured in Figure 4.1. We again consider a magnetic field in the negative x-direction, perpendicular to the band splitting b_z and the surface. Since we added a vacuum on the right side, we get two vacuum wavefunctions, as well as surface states on both surfaces of the semimetal.

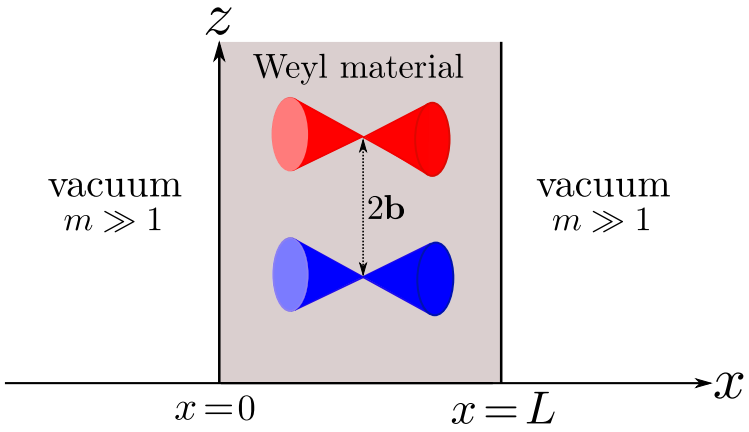

Figure 4.1 – Schematic picture of a model of a finite slab of Weyl semimetal bordered by a vacuum at $x = 0$ and $x = L$. Picture adapted from Ref. [1]

.

4.1 Surface state solutions

4.1.1 Solutions in semimetal bulk

In this case, we follow Section 3.3, but add another surface state on the right side of the semimetal. Again, we have the Hamiltonian

$$H = \epsilon \left[(-i\boldsymbol{\nabla} + e\mathbf{A}) \cdot \boldsymbol{\sigma} - \epsilon b_z \sigma_3 \right], \tag{4.1}$$

with the gauge $\mathbf{A} = (0, Bz, 0)$. Now that we have two surfaces (at $x = 0$ and $x = L$), we have surface states on the left and right side of the semimetal that

we have to consider. Our ansatz is now given by

$$|\psi_{\mathrm{SM}}(\vec{x})\rangle = e^{ik_y y}e^{-\lambda_0 x}\left[C_{0,1}\,|\psi_{0,1}\rangle + C_{0,2}\,|\psi_{0,-1}\rangle\right] +$$
$$e^{ik_y y}\sum_{n>0}\left(e^{-\lambda_n x}\left[C^{\ell}_{n,1}\,|\psi_{n,1}\rangle_{\ell} + C^{\ell}_{n,2}\,|\psi_{n,-1}\rangle_{\ell}\right] + e^{-\lambda_n(L-x)}\left[C^{r}_{n,1}\,|\psi_{n,1}\rangle_{r} + C^{r}_{n,2}\,|\psi_{n,-1}\rangle_{r}\right]\right),$$

where the ℓ,r lables surface states on the left and right of the material respectively. Similar to Chapter 3, we get

$$|\psi_{0,1}\rangle = \begin{pmatrix} e^{ib_z z}\,|0\rangle \\ 0 \\ 0 \\ 0 \end{pmatrix} \quad |\psi_{0,-1}\rangle = \begin{pmatrix} 0 \\ 0 \\ e^{-ib_z z}\,|0\rangle \\ 0 \end{pmatrix},$$

$$|\psi_{n,1}\rangle_{\ell} = \begin{pmatrix} a_{n,1}\;\; e^{ib_z z}\,|n\rangle \\ b_{n,1}\;\; e^{ib_z z}\,|n-1\rangle \\ 0 \\ 0 \end{pmatrix} \quad |\psi_{n,-1}\rangle_{\ell} = \begin{pmatrix} 0 \\ 0 \\ a_{n,-1}\;\; e^{-ib_z z}\,|n\rangle \\ b_{n,-1}\;\; e^{-ib_z z}\,|n-1\rangle \end{pmatrix},$$

where a_n,b_n are given by Eq. 2.21 with $k_x = -i\lambda_n$. The states on the right side of the semimetal $|\psi_n\rangle_r$ are found by substituting λ_n by $-\lambda_n$ in a_n and b_n.

4.1.2 Solutions in vacuum

In the vacuum we have the Hamiltonian

$$H = \gamma^0\left[\vec{\gamma}\cdot(-i\nabla + e\vec{A}) + im\right]$$

We make the ansatz for the wavefunction in the vacuum left of the semimetal

$$|\tilde{\psi}_{\ell}(\mathbf{x})\rangle = e^{ik_y y}\sum_n \tilde{c}_n e^{\tilde{\lambda}_n x}\,|\tilde{\psi}_n\rangle_{\ell},$$

where $|\tilde{\psi}_n\rangle_{\ell}$ are the Landau level states we found in the bulk, minus the phase from the splitting of the cones. Note that the wave function in the vacuum on the right is found by replacing x by $(L-x)$ and switching the sign of $\tilde{\lambda}_n$ in its eigenstates. Similar to Chapter 3, we get the eigenenergies

$$E_n = \pm\sqrt{2eBn + m^2 - \tilde{\lambda}_n^2}, \tag{4.2}$$

which we can again rewrite for $\tilde{\lambda}_n$

$$\tilde{\lambda}_n = \pm\sqrt{2eBn + m^2 - E^2}. \tag{4.3}$$

We discard the negative solution since it blows up for $x \to -\infty$ (and for $x \to \infty$ in the case of the surface state on the right). Solving the Schrödinger equation again gives the four solutions

$$|\tilde{\psi}_{n,1}\rangle_{\ell} = \frac{1}{\sqrt{2(2eBn+m^2)}}\begin{pmatrix} i\sqrt{2eBn}\,|n\rangle \\ (iE_n - \tilde{\lambda}_n)\,|n-1\rangle \\ 0 \\ m\,|n-1\rangle \end{pmatrix},$$
$$|\tilde{\psi}_{n,2}\rangle_{\ell} = \frac{1}{\sqrt{2(2eBn+m^2)}}\begin{pmatrix} (iE_n + \tilde{\lambda}_n)\,|n\rangle \\ i\sqrt{2eBn}\,|n-1\rangle \\ m\,|n\rangle \\ 0 \end{pmatrix}, \tag{4.4}$$

where E_n, given by Eq. 4.2, can be positive and negative. The solutions in the vacuum on the right are found by switching the sign of $\tilde{\lambda}_n$.

4.1.3 Matching

Now that we found the full wave functions in both sides of the vacuum and in the semimetal, we have to match them at the boundaries $x = 0$ and $x = L$. In the last two sections, we found the wave functions

$$|\psi_{\mathrm{SM}}(\vec{x})\rangle = e^{ik_y y}e^{-\lambda_0 x}\left[C_{0,1}\left|\psi_{0,1}\right\rangle + C_{0,2}\left|\psi_{0,-1}\right\rangle\right] +$$
$$e^{ik_y y}\sum_{n>0}\left(e^{-\lambda_n x}\left[C^{\ell}_{n,1}\left|\psi_{n,1}\right\rangle_{\ell} + C^{\ell}_{n,2}\left|\psi_{n,-1}\right\rangle_{\ell}\right] + e^{-\lambda_n(L-x)}\left[C^{r}_{n,1}\left|\psi_{n,1}\right\rangle_{r} + C^{r}_{n,2}\left|\psi_{n,-1}\right\rangle_{r}\right]\right)$$

$$|\tilde{\psi}_{\ell}(\mathbf{x})\rangle = e^{ik_y y}e^{-\tilde{\lambda}_0 x}\tilde{C}_0\begin{pmatrix}\frac{im}{\sqrt{2}(E+i\tilde{\lambda}_0)}\left|0\right\rangle\\ 0\\ \frac{1}{\sqrt{2}}\left|0\right\rangle\\ 0\end{pmatrix} + e^{ik_y y}\sum_{n=1}^{\infty}e^{-\tilde{\lambda}_n x}\left[\tilde{C}_{n,1}\left|\tilde{\psi}_{n,1}\right\rangle_{\ell} + \tilde{C}_{n,2}\left|\tilde{\psi}_{n,2}\right\rangle_{\ell}\right]$$
$$= e^{ik_y y}e^{-\tilde{\lambda}_0 x}\tilde{C}_0\left|\tilde{\psi}_0\right\rangle_{\ell} + e^{ik_y y}\sum_{n=1}^{\infty}e^{-\tilde{\lambda}_n x}\left[\tilde{C}_{n,1}\left|\tilde{\psi}_{n,1}\right\rangle_{\ell} + \tilde{C}_{n,2}\left|\tilde{\psi}_{n,2}\right\rangle_{\ell}\right],$$

where $\lambda_n = \sqrt{2eBn - E^2}$, $\tilde{\lambda}_n = -\sqrt{2eBn + m^2 - E^2}$ and $\tilde{\psi}_r(\mathbf{x})$ is given by $\tilde{\psi}_{\ell}(\mathbf{x})$ but with $e^{-\tilde{\lambda}_n(L-x)}$ and $\tilde{\lambda}_n \to -\tilde{\lambda}_n$ in the eigenstates. We now want to match these wave functions on the boundaries. We set $|\psi_{SM}(x=0)\rangle = |\tilde{\psi}_{\ell}(x=0)\rangle$ and $|\psi_{SM}(x=L)\rangle = |\tilde{\psi}_r(x=L)\rangle$. Again, we can project with vectors containing harmonic oscillator states from the left. Firstly, we can project with $(\langle n'|, 0, 0, 0)^T$. On the vacuum side this gives (for $|n'| > 0$)

$$\sum_n(\tilde{C}_{n,1}\tilde{a}_{n,1} + \tilde{C}_{n,2}\tilde{a}_{n,1})\langle n'|n\rangle = \tilde{C}_{n',1}\frac{i\sqrt{2eBn'}}{\sqrt{2(2eBn' + m^2)}} + \tilde{C}_{n',2}\frac{iE + \tilde{\lambda}_{n'}}{\sqrt{2(2eBn' + m^2)}}.$$

On the semimetal side, we have overlap with all states. Here we get

$$\sum_n C_{n,1}a_{n,1}\langle n'|e^{ib_z z}|n\rangle = \sum_n C_{n,1}a_{n,1}P_{n',n},$$

where $P_{n',n}$ is given by Eq. 3.33. Projecting for every n gives us the matrix equation

$$\begin{pmatrix}a_{0,1}P_{0,0} & a_{1,1}P_{0,1} & a_{2,1}P_{0,2} & \dots\\ a_{0,1}P_{1,0} & a_{1,1}P_{1,1} & a_{2,1}P_{1,2} & \\ a_{0,1}P_{2,0} & a_{1,1}P_{2,1} & a_{2,1}P_{2,2} & \\ \vdots & & & \ddots\end{pmatrix}\begin{pmatrix}C_{0,1}\\ C_{1,1}\\ C_{2,1}\\ \vdots\end{pmatrix} = \begin{pmatrix}\tilde{C}_0\tilde{a}_0\\ \tilde{C}_{1,1}\tilde{a}_{1,1} + \tilde{C}_{1,2}\tilde{a}_{1,2}\\ \tilde{C}_{2,1}\tilde{a}_{2,1} + \tilde{C}_{2,2}\tilde{a}_{2,2}\\ \vdots\end{pmatrix}.$$

Projecting on the vectors

$$\begin{pmatrix}0\\ \langle n'|\\ 0\\ 0\end{pmatrix}, \begin{pmatrix}0\\ 0\\ \langle n'|\\ 0\end{pmatrix}, \begin{pmatrix}0\\ 0\\ 0\\ \langle n'|\end{pmatrix}$$

also each give a set of equations. Furthermore, we require normalization of the entire wavefunction

$$\int_{-\infty}^{0}\mathrm{d}x|\psi_l(\mathbf{x})|^2 + \int_0^L \mathrm{d}x|\psi_{\mathrm{SM}}(\mathbf{x})|^2 + \int_L^{\infty}\mathrm{d}x|\psi_r(\mathbf{x})|^2 = 1.$$

In this case, if we take Landau levels into account up to the n-th level, we have $4 + 8n$ coefficients plus the energy, giving a total of $5 + 8n$ unknowns. By including the surface on the right, we added equations from the matching on the right, giving a total of $5 + 8n$ equations. That means we are able to solve the system, showing that there are surface state solutions in a finite slab of Weyl semimetal.

We showed that cutting off at a certain level n gives us a solvable system. However, this problem becomes infinitely large, as we can include infinitely many Landau levels. Consequently, we need to use some cutoff at a certain Landau level to be able to solve the problem. However, since we have energies $E_n = \sqrt{2eBn - \lambda_n^2}$ for $n > 0$ and $E_0 = -\epsilon i \lambda_0$, the Landau level energy spacing is close to $\sqrt{2eB}$. For low magnetic fields, the energy spacing is small and the Landau levels almost lie on top of eachother. That means there is no reasonable cutoff that we can use to solve the system. However, the problem can be solved in the high magnetic field limit, where the energy spacing becomes much bigger.

4.2 LLL limit

The solutions we found in the bulk contained a linear combination of Landau levels, with energy separation $\Delta E \propto \sqrt{B}$. For low magnetic fields, we cannot throw away most these Landau levels because they are so close in energy. However, the lowest Landau level has a constant energy in B, $E = \epsilon k_x$. Therefore, if we take the high magnetic field limit, we can assume that for low energies, this is the only Landau level in the bulk that we have to take into account. We also call this the lowest Landau level limit (LLL limit). This limit is often used in physics using Landau levels, such as the Fractional Quantum Hall effect [23] and rotating Bose condensates [24]. If we lower the magnetic field such that also the first Landau level can contribute, we can find first order corrections to this limit. However, as we will see, this already increases the complexity of the problem enough to force us to use numerics.

In the LLL limit, we neglect any states higher than the lowest Landau level (LLL). In the semimetal, the zeroth level, although not being a surface state, contributes to the problem. It has two states, one in each cone, propagating through the semimetal. These states are chiral, their propagation direction is determined by their chirality $\epsilon = \pm 1$. On the vacuum side we have only one state

in the zeroth Landau level. We have the wavefunctions

$$|\tilde{\psi}_\ell(\mathbf{x})\rangle = Ae^{ik_y y}e^{-\tilde{\lambda}_0 x}\begin{pmatrix} \frac{im}{\sqrt{2}(E+i\tilde{\lambda}_0)}|0\rangle \\ 0 \\ \frac{1}{\sqrt{2}}|0\rangle \\ 0 \end{pmatrix}$$

$$|\tilde{\psi}_r(\mathbf{x})\rangle = De^{ik_y y}e^{-\tilde{\lambda}_0 (L-x)}\begin{pmatrix} \frac{im}{\sqrt{2}(E-i\tilde{\lambda}_0)}|0\rangle \\ 0 \\ \frac{1}{\sqrt{2}}|0\rangle \\ 0 \end{pmatrix}$$

$$|\psi_{\mathrm{SM}}(\mathbf{x})\rangle = e^{ik_y y}\left[Be^{iEx}\begin{pmatrix} e^{ib_z z}|0\rangle \\ 0 \\ 0 \\ 0 \end{pmatrix} + Ce^{-iEx}\begin{pmatrix} 0 \\ 0 \\ e^{-ib_z z}|0\rangle \\ 0 \end{pmatrix}\right],$$

where $\tilde{\lambda}_0 = -\sqrt{m^2 - E^2}$ and A, B, C, D and the energy E are to be determined by matching the wave functions. Note that in the vacuums we have exponentially decaying wave functions, whereas in this limit we have a propagating wave function in the semimetal. The direction of propagation depends on the chirality of the state. Looking at the wave functions, we can see why an infinite slab of Weyl semimetal does not give solutions for the surface states. In that case we only have ψ_ℓ and ψ_{SM}, which have three unknowns plus the energy. To get the equations to solve the matching problem, we can project with two vectors from the left to get two equations. Adding the normalization of the wave function adds one equation, which gives a total of three equations for four unknowns. However, if we consider a finite slab of Weyl metal and add the vacuum on the right, we add two equations from matching on the right side, but only one unknown D. In total we have five equations and five unknowns, so we can solve the system. We were also inspired by Ref. [25], where the authors use a semiclassical calculation on this system. They find that a lot of the properties of the magnetic orbits they find depend on the length of the material L. Therefore, we considered a finite slab, hoping to find the same dependence on the length L.

We first match the wavefunctions of the left vacuum and the semimetal at $x = 0$.
We project with $(\langle 0|, 0, 0, 0)$ and $(0, 0, \langle 0|, 0)$ to get the equations

$$B = \frac{im}{\sqrt{2}(E + i\tilde{\lambda}_0)}e^{b_z^2/4eB + ib_z k_y/eB}A$$
$$C = \frac{1}{\sqrt{2}}e^{b_z^2/4eB - ib_z k_y/eB}A.$$

Secondly, we match the wavefunctions of the vacuum on the right and the semimetal at $x = L$. This gives the equations

$$B = \frac{im}{\sqrt{2}(E - i\tilde{\lambda}_0)}e^{-iEL}e^{b_z^2/4eB + ib_z k_y/eB}D$$
$$C = \frac{1}{\sqrt{2}}e^{iEL}e^{b_z^2/4eB - ib_z k_y/eB}D.$$

Comparing the results for C, we get

$$A = e^{iEL}D. \tag{4.5}$$

When we compare the results for B, we find

$$A = e^{-iEL}\frac{E + i\tilde{\lambda}_0}{E - i\tilde{\lambda}_0}D. \tag{4.6}$$

Combining Eqs 4.5 and 4.6 gives the equation

$$e^{iEL} = e^{-iEL}\frac{E + i\tilde{\lambda}_0}{E - i\tilde{\lambda}_0}.$$

We take the log on both sides to get

$$2iEL = \log\left(\frac{E + i\sqrt{m^2 - E^2}}{E - i\sqrt{m^2 - E^2}}\right) = 2i\arctan\left(\frac{\sqrt{m^2 - E^2}}{E}\right) + q\pi,$$

where the integer $q \in (-\infty, \infty)$. We have to add these copies of the arctan since one copy of the arctan is restricted vertically between $-\pi/2$ and $\pi/2$, while $\tan(x)$ has values in the whole domain $x \in (-\infty, \infty)$. So our equation for the energy is

$$EL = \arctan\left(\frac{\sqrt{m^2 - E^2}}{E}\right) + q\pi. \tag{4.7}$$

This has no known closed form solutions. The argument is defined for $|E| \leq m$, so the two functions have a finite amount of intersections for finite m and L. The amount of positive and negative energy solutions is equal by particle-hole symmetry.

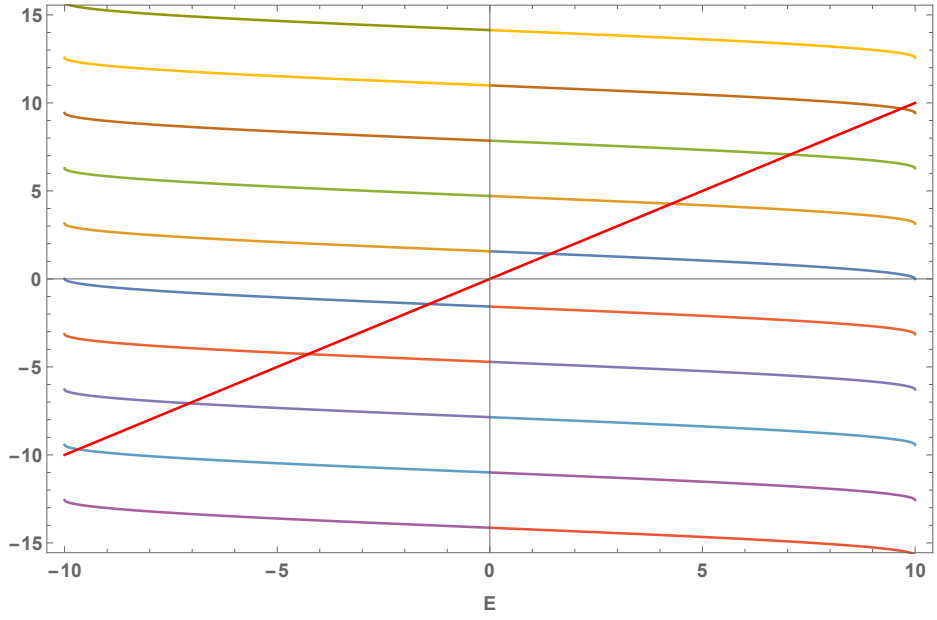

Figure 4.2 – The two functions for varying E, with $L = 1, m = 10$. Different colours represent different branches of the arctan. The intersections mark allowed energies of the system. There are 8 solutions in this case (4 positive, 4 negative).

For instance, for $L = 1, m = 10$ we get 4 positive energy solutions and 4 negative energy solutions. The first q for which there is no intersection is given by the equation $mL < \pi q$. We find that the largest q for which there is an intersection is given by $q_{max} = \lceil \frac{mL}{\pi} \rceil - 1$.

4.2.1 Normalization of the wavefunction

We have the normalization condition

$$\int_{\infty}^{0} \mathrm{d}x|\psi_\ell(x)|^2 + \int_0^L \mathrm{d}x|\psi_{\mathrm{SM}}(x)|^2 + \int_L^{\infty} \mathrm{d}x|\psi_r(x)|^2 = 1$$
$$= \frac{|A|^2}{2\sqrt{m^2-E^2}} + (|B|^2+|C|^2)L + |D|^2\frac{e^{-2\sqrt{m^2-E^2}}}{2\sqrt{m^2-E^2}}.$$

We can express all the coefficients in terms of D. Solving for D gives

$$D = \pm\left[\frac{1+e^{-2\sqrt{m^2-E^2}L}}{2\sqrt{m^2-E^2}} + Le^{\frac{b_z^2}{2eB}}\right]^{-1/2}.$$

We choose the + solution for D. The wavefunction is now known everywhere. It is given by

$$|\tilde{\psi}_\ell(\mathbf{x})\rangle = De^{ik_y y}e^{iEL}e^{-\tilde{\lambda}_0 x}\begin{pmatrix}\frac{im}{\sqrt{2}(E+i\tilde{\lambda}_0)}|0\rangle\\0\\\frac{1}{\sqrt{2}}|0\rangle\\0\end{pmatrix},$$

$$|\tilde{\psi}_r(\mathbf{x})\rangle = De^{ik_y y}e^{-\tilde{\lambda}_0(L-x)}\begin{pmatrix}\frac{im}{\sqrt{2}(E-i\tilde{\lambda}_0)}\\0\\\frac{1}{\sqrt{2}}|0\rangle\\0\end{pmatrix},$$

$$|\psi_{\mathrm{SM}}(\mathbf{x})\rangle = \frac{im}{\sqrt{2}(E-i\tilde{\lambda}_0)}De^{ik_y y}e^{iE(x-L)}e^{b_z^2/4eB+ib_z k_y/eB}\begin{pmatrix}e^{ib_z z}|0\rangle\\0\\0\\0\end{pmatrix}$$

$$+\frac{1}{\sqrt{2}}De^{ik_y y}e^{iE(L-x)}e^{b_z^2/4eB-ib_z k_y/eB}\begin{pmatrix}0\\0\\e^{-ib_z z}|0\rangle\\0\end{pmatrix}.$$

4.2.2 $m \to \infty$ limit

If we take the $m \to \infty$ limit we can get analytic solutions for the energy. In this limit the arctan becomes a step-function: $\lim_{m\to\infty}\arctan\left(\frac{\sqrt{m^2-E^2}}{E}\right) = \mathrm{sgn}(E)\frac{\pi}{2}$. The equation for the energy Eq. 4.7, then becomes very simple.

$$EL = \frac{\pi}{2} + n\pi.$$

So the energy is

$$E = \frac{\pi}{L}\left(q+\frac{1}{2}\right), \tag{4.8}$$

giving $\Delta E = \frac{\pi}{L}$. In SI units, the energy is given by

$$E = \hbar v_F\frac{\pi}{L}\left(q+\frac{1}{2}\right). \tag{4.9}$$

This result is in agreement with the numerically obtained result in Ref. [26] and semiclassically obtained in Ref. [25] where they find (for $\hbar, v_F \equiv 1$)

$$E = \frac{\pi(q+\gamma)}{L + b_z l_b^2}. \tag{4.10}$$

In the high magnetic field limit we can neglect the second term in the denominator and get our result with $\gamma = \frac{1}{2}$. We find that the phase shift $\gamma = \frac{1}{2}$ agrees with what is found numerically in Ref. [26].

The eigenvectors become much simpler in this limit. The surface states decay with $e^{-\sqrt{m^2-E^2}}$, so in this limit the vacuum wavefunction is zero outside the surface. The wavefunction becomes

$$|\tilde{\psi}_\ell(x=0)\rangle = \frac{1}{\sqrt{2L}} e^{-b_z^2/4eB} e^{ik_y y} e^{iEL} \begin{pmatrix} |0\rangle \\ 0 \\ |0\rangle \\ 0 \end{pmatrix}$$

$$|\tilde{\psi}_r(x=L)\rangle = \frac{1}{\sqrt{2L}} e^{-b_z^2/4eB} e^{ik_y y} \begin{pmatrix} -|0\rangle \\ 0 \\ |0\rangle \\ 0 \end{pmatrix}$$

$$|\psi_{\mathrm{SM}}(\mathbf{x})\rangle = \frac{e^{ik_y y}}{\sqrt{2L}} \left[-e^{iE(x-L)} e^{ib_z(z+k_y/eB)} \begin{pmatrix} |0\rangle \\ 0 \\ 0 \\ 0 \end{pmatrix} + e^{iE(L-x)} e^{-ib_z(z+k_y/eB)} \begin{pmatrix} 0 \\ 0 \\ |0\rangle \\ 0 \end{pmatrix} \right].$$

This result shows that the wave function still has a spin structure on the surfaces. That means we could not have found the same result using the boundary conditions $\psi = 0$ on the surfaces. In fact, it was necessary to start at a finite mass to find the correct wave functions, before taking the limit $m \to \infty$. We see that the wave function in the semimetal goes as $e^{iEx} = e^{i\frac{\pi}{L}(n+\frac{1}{2})x}$. The energy of these chiral modes is thus determined by the number of nodes n the wave function has in the metal. In the semiclassical description in Ref. [25], the authors describe these modes as an electron moving through the Weyl metal (see Figure 4.3). Note that they have their axes switched compared to ours, such that the orbits go from bottom to top instead of left to right. The chiral mode is described as an electron on the negative chirality Weyl node on the bottom surface sliding along the Fermi arc towards positive chirality Weyl node. It then moves through the bulk towards the positive chirality Weyl node on the top and slides along the Fermi arc to the negative Weyl node. Finally, moving through the bulk again, it completes its orbit. This chiral mode acts as a one-way "conveyor belt", moving electrons from surface to surface. These quantized magnetic orbits turn out to produce quantum oscillations. Very recently, in Ref. [27], experimental signatures of these orbits have been found, where it is dubbed the "topological sink effect".

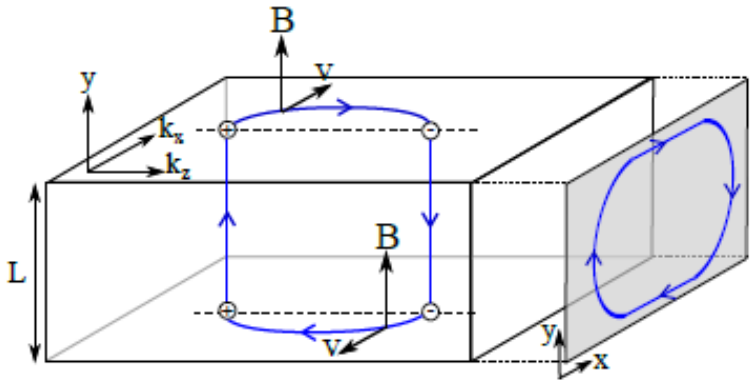

Figure 4.3 – Schematic picture of quantized magnetic orbits going through the bulk to the Weyl nodes. Note that in this picture the x and y axis are switched compared to our setup. Picture taken from Ref. [25].

We have now solved the full surface state problem in the high magnetic field limit. Using these results we can study the effects of the anomalous magnetic moment in this limit.

4.3 Anomalous effects

The Rashba-spin-orbit term has already been investigated further in Ref. [1], so we focus on the anomalous Zeeman term and the tilt terms in Eq. 1.14 that follow from the anomalous magnetic moment calculation. First, we treat the terms separately. Then, we combine them and show that we can also understand this result using the fact that the lowest Landau level is spin-polarized.

4.3.1 Zeeman term

For a magnetic field in the negative x-direction, the contribution of the Zeeman term to the Hamiltonian is given by $\mu_2\sigma_1 B$. The full Hamiltonian with this term added is given by

$$H = \epsilon\left[(-i\boldsymbol{\nabla} + e\mathbf{A} - \epsilon\mathbf{b} - \epsilon\mu_2\mathbf{B})\cdot\boldsymbol{\sigma}\right] \tag{4.11}$$

Using the ansatz for the unperturbed problem

$$\begin{aligned}|\psi_{\mathrm{SM}}(\mathbf{x})\rangle &= e^{ik_y y}e^{\lambda_0 x}\left[C_{0,1}\left|\psi_{0,1}\right\rangle + C_{0,2}\left|\psi_{0,-1}\right\rangle\right] + \\ e^{ik_y y}\sum_n &\left(e^{\lambda_n x}\left[C^{\ell}_{n,1}\left|\psi_{n,1}\right\rangle_{\ell} + C^{\ell}_{n,2}\left|\psi_{n,-1}\right\rangle_{\ell}\right] + e^{\lambda_n(L-x)}\left[C^{r}_{n,1}\left|\psi_{n,1}\right\rangle_{r} + C^{r}_{n,2}\left|\psi_{n,-1}\right\rangle_{r}\right]\right),\end{aligned} \tag{4.12}$$

we find that the Schrödinger equation for the n-th level gives

$$\epsilon\left[\sigma_1(\pm i\lambda_n + \epsilon\mu_2 B) + \sigma_2(k_y + eBz) + \sigma_3(-i\partial_z - \epsilon b_z)\right]\left|\psi_{n,\epsilon}\right\rangle = E\left|\psi_{n,\epsilon}\right\rangle,$$

where the left states give $+i\lambda_n$ and the right states $-i\lambda_n$. We see that the Zeeman term shifts λ_n in a chirality dependent way as $\lambda_n \to \lambda_n \mp \epsilon i\mu_2 B$. Therefore, we

change our ansatz to include this shift. Our new ansatz is

$$
\begin{aligned}
|\psi_{\mathrm{SM}}(\vec{x})\rangle &= e^{ik_y y}\left[C_{0,1}e^{(iE-i\mu_2 B)x}\,|\psi_{0,1}\rangle + C_{0,2}e^{-(iE-i\mu_2 B)x}\,|\psi_{0,2}\rangle\right] \\
&+ e^{ik_y y}\sum_n \left[C^{\ell}_{n,1}e^{(-\lambda_n-\epsilon i\mu_2 B)x}\,|\psi_{n,1}\rangle_\ell + C^{\ell}_{n,2}e^{(-\lambda_n-\epsilon i\mu_2 B)x}\,|\psi_{n,2}\rangle_\ell\right. \\
&\left.+ C^{r}_{n,1}e^{(\lambda_n-\epsilon i\mu_2 B)(x-L)}\,|\psi_{n,1}\rangle_r + C^{r}_{n,2}e^{(\lambda_n-\epsilon i\mu_2 B)(x-L)}\,|\psi_{n,2}\rangle_r\right].
\end{aligned}
$$

Now applying the Hamiltonian to $|\psi_{n,\epsilon}\rangle$ gives the same eigenenergy $E = \pm\sqrt{2eBn - \lambda_n^2}$. However, we changed the wavefunction, so through the matching problem the energy of the surface state may be different.

When we go through the matching problem again with the new wavefunction, we find that the matching at the right side of the metal at $x = L$ is slightly different. The lowest Landau-level wave function in the semimetal is now

$$
|\psi_{SM}(\vec{x})\rangle = e^{ik_y y}\left[C_{0,1}e^{iEx-i\mu_2 Bx}e^{ib_z z}\begin{pmatrix}|0\rangle\\0\\0\\0\end{pmatrix} + C_{0,2}e^{-iEx+i\mu_2 Bx}e^{-ib_z z}\begin{pmatrix}0\\0\\|0\rangle\\0\end{pmatrix}\right].
$$

At $x = L$, we also get the contribution $-i\mu_2 BL$ in the exponential. The equation that determines the energy is now given by

$$
e^{iL(E-\mu_2 B)} = e^{-iL(E-\mu_2 B)}\frac{E+i\tilde{\lambda}_0}{E-i\tilde{\lambda}_0}.
$$

When we take the log we get

$$
EL - \mu_2 BL = \arctan\left(\frac{\sqrt{m^2-E^2}}{E}\right) + q\pi.
$$

In the $m \to \infty$ limit this gives the energy

$$
E = \frac{\pi}{L}\left(q+\frac{1}{2}\right) + \mu_2 B. \tag{4.13}
$$

Thus, the energy is shifted by $\mu_2 B$, as is usual for a Zeeman effect. In SI units, Eq. 4.13 is given by

$$
E = \hbar v_F \frac{\pi(q+\frac{1}{2})}{L} + \mu_2 B. \tag{4.14}
$$

For the typical values $B = 10\ T$, $L = 100$ nm, $v_F = c/300$, $\mu_2 = 0.85\mu_B$ [1], we find that the first term is of the order $\hbar v_f/L \propto 10^{-19}$, while the second term is of the order $\mu_2 B \propto 10^{-23}$. The change of the energy due to the anomalous Zeeman effect for $B = 10T$ is about 1 in 10.000.

4.3.2 Tilt term

The tilt term goes as $\epsilon\mu_1 \mathbf{k}\cdot\mathbf{B}$. In the semimetal, we have to add to the Hamiltonian $H_{\mathrm{tilt}} = \epsilon\mu_1(\mathbf{k}\cdot\mathbf{B})\mathbf{1}_2$, giving the full Hamiltonian

$$
H = \epsilon\left[(-i\boldsymbol{\nabla} + e\mathbf{A} - \epsilon\mathbf{b})\cdot\boldsymbol{\sigma} + \mu_1(\mathbf{k}\cdot\mathbf{B})\mathbf{1}_2\right]
$$

Again using the ansatz (4.12) for the undisturbed problem , we find that the eigenenergies are now given by $E = \sqrt{2eBn - \lambda_n^2} + i\epsilon\mu_1 B\lambda_n$ for $n > 0$. Writing λ again in terms of E, we find

$$\lambda_n = \frac{1}{1-\mu_1^2 B^2}\left(\epsilon i\mu_1 BE \pm \sqrt{2eBn(1-\mu_1^2 B^2) - E^2}\right).$$

We find that λ_n always contains an imaginary part. This means that even exponentially decaying Landau levels get an oscillating part in their states. We have two cases, $\mu_1^2 B^2 < 1$ and $\mu_1^2 B^2 > 1$. In the first case, we have an imaginary part and a real part of λ_n. We choose the plus sign for the real part to get a surface state, since then $Re[\lambda_n] > 0$. In this case we still have a surface state, however it is oscillating. In the second case, $\mu_1^2 B^2 > 1$, the square root becomes negative which means that λ_n becomes completely imaginary. This case is depicted in Figure 4.4, where the cones have tilted so much that they are back at the Fermi level, creating a Fermi sea. This is called a type-II Weyl semimetal [28]. We use the parameters as chosen in Ref. [1], $\frac{\mu_1 k_F}{\mu_B} \approx 0.25$ with $k_F = 0.04\mathring{A}^{-1}$. In SI units the condition is given by $\mu_1^2 B^2 > \hbar^2 v_F^2$. Using these numbers and $v_F = c/300$, we find a critical magnetic field of approximately $18000T$, which is unrealistic. We conclude from this that the anomalous tilting effect is not enough to transition a type-I Weyl semimetal to a type-II Weyl semimetal. The type-II Weyl semimetals already have a tilted band structure at $B = 0$, where the anomalous effects vanish.

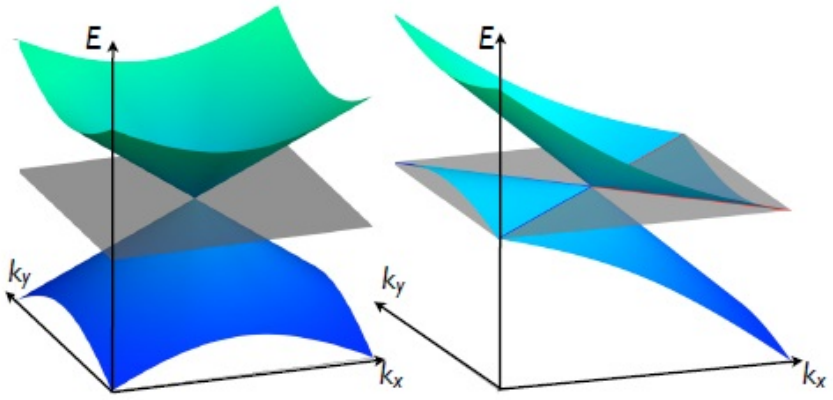

Figure 4.4 – A single Weyl cone for an untilted type-I Weyl semimetal (left) and a tilted type-II Weyl semimetal (right). The Fermi surface for a type-II semimetal is no longer a point and contains electron and hole states. Picture taken from Ref. [28].

In the high magnetic field limit, we just have to take the lowest Landau level in account. In this case the effect of the tilt term is easy to describe. The lowest Landau level is chiral and its energy is given by $E = \epsilon k_x$. For the surface states this means we get $E = -i\epsilon\lambda_0$, giving $\lambda_0 = \epsilon iE$. When we add the tilt term we get $E = -i\epsilon\lambda_0 - i\epsilon\mu_1 B\lambda_0$. This gives a rescaled λ_0, as we get $\lambda_0 = \frac{\epsilon iE}{1+\mu_1 B}$. The effect on the energies is simple, as our equation for the energy now becomes

$$\frac{EL}{1+\mu_1 B} = \arctan\left(\frac{\sqrt{m^2 - E^2}}{E} + q\pi\right),$$

which in the $m \to \infty$ limit gives

$$E = \frac{\pi(q+\frac{1}{2})}{L}(1+\mu_1 B). \tag{4.15}$$

In SI units 4.15 becomes

$$E = \frac{\pi(q+\frac{1}{2})}{L}(\hbar v_F + \mu_1 B). \tag{4.16}$$

We see that the tilt term rescales the Fermi velocity in the LLL limit. Using the typical values as before, together with Fermi momentum $k_F = 0.04\mathring{A}^{-1}$ [1], we find that the Fermi velocity is increased by about 55 m/s, which on a total of 10^6 m/s is about a 1 in 20.000 change.

4.3.3 Spin polarization

The above results in the LLL limit could also have been obtained by observing that the lowest Landau level is spin-polarized in the x-direction. Since the spins are always in the x-direction, we can set $\sigma_x = 1$ since we essentially have a 1-dimensional spin space. We can use this observation to greatly simplify the problem. We have the Hamiltonian

$$H = \epsilon\left[\sigma_1(-i\lambda_0 + \epsilon\mu_2 B) + \sigma_2(k_y + eBz) + \sigma_3(-i\partial_z + \epsilon b_z) - i\lambda_0\mu_1 B\right].$$

Since we set $\sigma_1 = 1$, we can add or remove this matrix structure as we like. We first change the spin-basis to the basis in which we solved the problem. We get

$$\tilde{H} = V^\dagger H V = \epsilon\begin{pmatrix} -i\lambda_0 & \sqrt{2eB}a^\dagger \\ \sqrt{2eB}a & i\lambda_0 \end{pmatrix} + V^\dagger\sigma_1\mu_2 B V - V^\dagger i\lambda_0\mu_1 B V,$$

where V is given in Eq. 2.16. Now we remove the σ_1 from the $\mu_2 B$ term and add it to the $\mu_1 B$ term. This gives

$$\begin{aligned}\tilde{H} &= \epsilon\begin{pmatrix} -i\lambda_0 & \sqrt{2eB}a^\dagger \\ \sqrt{2eB}a & i\lambda_0 \end{pmatrix} + \mu_2 B - i\lambda_0\mu_1 B V^\dagger\sigma_1 V \\ &= \epsilon\begin{pmatrix} -i\lambda_0(1+\epsilon\mu_1 B) & \sqrt{2eB}a^\dagger \\ \sqrt{2eB}a & i\lambda_0(1+\epsilon\mu_1 B) \end{pmatrix} + \mu_2 B,\end{aligned}$$

since $V^\dagger\sigma_1 V = \begin{pmatrix} 1 & 0 \\ 0 & -1 \end{pmatrix}$. Solving for the eigenenergies we get (in SI units)

$$E = -i\epsilon\hbar v_F(1+\epsilon\mu_1 B) + \mu_2 B,$$

so we see that the Fermi velocity is rescaled with $\mu_1 B$ in the propagation direction (determined by ϵ). Now that we know this, we can skip the matching problem and simply rescale the Fermi velocity and add the $\mu_2 B$ term in our previous result. Therefore the energy of the surface state is given by

$$E = \hbar v_F(1+\mu_1 B)\frac{\pi(q+\frac{1}{2})}{L} + \mu_2 B.$$

4.4 Corrections on the LLL limit

We now consider the problem with two Landau levels, the zeroth level we included above and the first Landau level (referred to as TLL). This amounts to lowering the magnetic field such that through thermal fluctuations the system can access the first Landau level but not the levels above. This is not a great approximation, as the energy levels only differ by approximately a factor $\sqrt{2}$. Still, this will help us understand what including another Landau level adds to the problem.

Note that we assume that the magnetic field is still large enough such that $b_z l_b^2 \ll 1$. We need this to guarantee that we are still in the limit where we have discretization of the energy. Recall that for $B = 0$, the surface state wave function is localized in momentum space between $-b_z$ and b_z. That means the wave function in real space is localized with length $1/b_z$. The magnetic field defines the magnetic length l_B, which has to be small compared to b_z for the wave function to 'feel' the magnetic field. We see this in the vacuum wave functions in the LLL limit, where the wave functions are localized by $e^{-b_z/4eB}$. This gives the condition $b_z l_b^2 \ll 1$.

Including the first Landau level, we get the wavefunctions

$$
\begin{aligned}
&|\psi_{\mathrm{SM}}(\mathbf{x})\rangle = e^{ik_y y} e^{\lambda_0 x} \left[C_{0,1} |\psi_{0,1}\rangle + C_{0,2} |\psi_{0,-1}\rangle\right] + \\
&e^{ik_y y} \left(e^{-\lambda_1 x} \left[C^{\ell}_{1,1} |\psi_{1,1}\rangle_{\ell} + C^{\ell}_{1,2} |\psi_{1,-1}\rangle_{\ell}\right] + e^{-\lambda_1 (L-x)} \left[C^{r}_{1,1} |\psi_{1,1}\rangle_{r} + C^{r}_{1,2} |\psi_{1,-1}\rangle_{r}\right] \right), \\
&|\tilde{\psi}_{\ell}(\mathbf{x})\rangle = e^{ik_y y} e^{-\tilde{\lambda}_0 x} \tilde{C}_0 |\tilde{\psi}_0\rangle_{\ell} + e^{ik_y y} \sum_{n=1}^{\infty} e^{-\tilde{\lambda}_n x} \left[\tilde{C}_{n,1} |\tilde{\psi}_{n,1}\rangle_{\ell} + \tilde{C}_{n,2} |\tilde{\psi}_{n,2}\rangle_{\ell}\right], \\
&|\tilde{\psi}_{r}(\mathbf{x})\rangle = e^{ik_y y} e^{-\tilde{\lambda}_0 (L-x)} \tilde{C}_0 |\tilde{\psi}_0\rangle_{r} + e^{ik_y y} \sum_{n=1}^{\infty} e^{-\tilde{\lambda}_n (L-x)} \left[\tilde{C}_{n,1} |\tilde{\psi}_{n,1}\rangle_{r} + \tilde{C}_{n,2} |\tilde{\psi}_{n,2}\rangle_{r}\right],
\end{aligned}
$$

where $\tilde{\lambda}_0 = -\sqrt{m^2 - E^2}$, $\tilde{\lambda}_1 = -\sqrt{2eB + m^2 - E^2}$, $\lambda_1 = \sqrt{2eB - E^2}$. The states $|\tilde{\psi}_n\rangle$ are given in 4.4. We now have 12 coefficients plus the energy we have to fix by matching the wave functions. We get 6 equations on each side of the semimetal, since we can project with the vectors

$$
\begin{pmatrix} \langle 0| \\ 0 \\ 0 \\ 0 \end{pmatrix}, \begin{pmatrix} 0 \\ \langle 0| \\ 0 \\ 0 \end{pmatrix}, \begin{pmatrix} 0 \\ 0 \\ \langle 0| \\ 0 \end{pmatrix}, \begin{pmatrix} 0 \\ 0 \\ 0 \\ \langle 0| \end{pmatrix}, \begin{pmatrix} \langle 1| \\ 0 \\ 0 \\ 0 \end{pmatrix}, \begin{pmatrix} 0 \\ 0 \\ \langle 1| \\ 0 \end{pmatrix}.
$$

We also have the normalization of the wavefunction, so we have as many equations as unknowns. In fact, each added level adds 4 coefficients in the semimetal and 2 coefficients in each vacuum that we have to match. There are also 8 more equations since we can now project with 4 more states on each surface. That means we can keep adding levels and get a solvable system, however the problem grows with 8 more equations and unknowns to solve per level.

To solve the problem at hand we have to set the determinant of a 12 by 12 matrix to zero and solve for the energy. The determinant function is fairly complicated, so we have to resort to numerics to find zeroes of this function. The zeroes of this function are the allowed energies. Looking at the energy difference between the simulated TLL and the LLL energy we find that the energy difference

falls off for high magnetic fields as expected. Consequently, we expect the energy to be similar to the result in the high magnetic field limit $E = \pi(n + \frac{1}{2})/L$, but with an extra term in the denominator as in Ref. [26], where they find

$$E = \frac{\pi(n + \gamma(B))}{L + b_z l_B^2}. \tag{4.17}$$

We make the assumption that this is the correct energy and try to check if it matches our numerical result. We define the dimensionless energy

$$\frac{EL}{\hbar v_F} = \frac{(n + \gamma(B))\pi}{1 + \frac{b_z}{L} l_B^2} = \frac{(n + \gamma(B))\pi}{1 + \bar{b}_z/\beta}, \tag{4.18}$$

Since the limit $B \to \infty$ should give us back the result we found in the LLL limit, we assume γ to be

$$\gamma = 1/2 + \varphi(b_z)/\beta, \tag{4.19}$$

where $\varphi(b_z)$ is the b_z dependence of γ, which we determine first. To find this we use the $n = 0$ energy of the TLL, $E_0 = \gamma\pi/(1 + \bar{b}_z/\beta)$. We multiply out all the irrelevant terms to get

$$\frac{E_0(1 + \bar{b}_z/\beta)}{\pi} = \gamma = \frac{c\varphi(\bar{b}_z)}{\beta} + \frac{1}{2}.$$

We substract the $\frac{1}{2}$ and multiply by β to get

$$\left(\gamma - \frac{1}{2}\right)\beta = \frac{E_0(1 + \bar{b}_z/\beta)\beta}{\pi} = c\varphi(\bar{b}_z).$$

Varying $\bar{b}_z$, we find that $\varphi(\bar{b}_z) = \bar{b}_z$. This means that we get

$$\gamma = \frac{1}{2}(1 + \frac{c\bar{b}_z}{\beta})$$

as our approximation. For $b_z = 1$ we can calculate this quantity and find c. Since our assumption of the correct energy is not perfect, c will still depend on the magnetic field slightly. Our assumption becomes more accurate the higher the magnetic field since we know γ should go to $\frac{1}{2}$. Therefore c should go to a constant for high magnetic fields. This is indeed the case, as c converges to $\frac{1}{2}$ for high magnetic fields. We put this into our assumption for the energy and compare to the numerically simulated result in Figure 4.5. The result approximates the simulated energy reasonably.

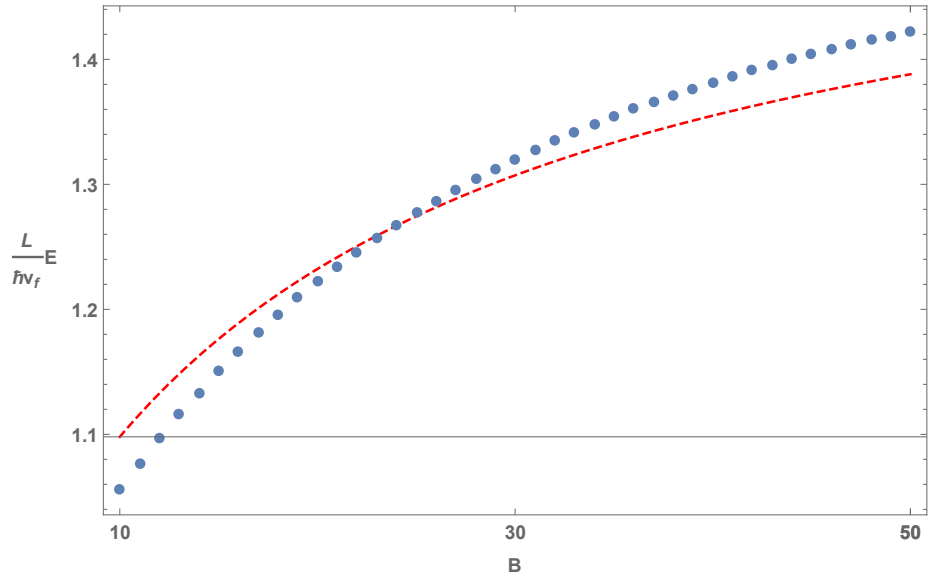

Figure 4.5 – The numerically simulated energy as a function of B (blue) compared to the approximation found using our assumption for γ with $c = \frac{1}{2}$ (red). The error of our approximation is about 1%.

To conclude, adding a Landau level gives the first-order correction in B to the energy

$$\frac{L}{\hbar v_F} E = \frac{\pi\left(q + \frac{1}{2}(1 + \frac{\bar{b_z}}{\beta})\right)}{1 + \frac{\bar{b_z}}{\beta}} = \frac{\pi\left(q + \frac{1}{2}(1 + \frac{b_z \hbar}{eBL})\right)}{1 + \frac{b_z \hbar}{eBL}}, \tag{4.20}$$

which vanishes for high magnetic fields. For the sake of accuracy, it is not completely correct to call this the first order correction. By approximation, we have only taken into account the first Landau level, while the energy separation of the levels is small. Adding multiple levels would probably add more $1/B$ corrections, but their magnitude should be small compared to the influence of the first Landau level. Therefore, this is the main contribution to the first order correction in B to the energy.

In this Chapter, we found solutions for surface states on a Weyl semimetal in a strong perpendicular magnetic field. Analytical solutions were found when we only considered the lowest Landau level to contribute. We derived that closed magnetic orbits with discrete energy levels are possible due to chiral modes propagating through the bulk. Next, we investigated the anomalous effects on these magnetic orbits and found that the energies were Zeeman shifted and the Fermi velocity rescaled. Finally we showed that, using numerics, we can also consider slightly lower magnetic fields by adding more Landau levels. We added one Landau level and found an approximation of the first order correction in the magnetic field to the energy of the LLL limit.

Chapter 5

Discussion

5.1 Summary

In this Thesis we investigated the effect of magnetic fields on the surface states of a slab of Weyl semimetal in a vacuum. We considered a time reversal symmetry broken semimetal by splitting the Weyl cones in momentum space with $\mathbf{b} = (0, 0, b_z)$. In Chapter 2, we found the Landau level solutions in the bulk of the Weyl semimetal for two cases. In the first case, we treated a magnetic field parallel to the surface and band splitting, and find Landau level eigenstates in the form of spinors of harmonic oscillator states. The band splitting b_z simply shifted the momentum k_z, giving energy levels (in SI units)

$$E_n = \hbar v_F \pm \sqrt{2eBn + (k_z - \epsilon b_z)^2}.$$

In the second case we treated a magnetic field perpendicular to the surface and band splitting. We find similar Landau level eigenstates except that in this case, the band splitting b_z generated a phase $e^{ib_z z}$ in front of the harmonic oscillator wave functions. The energies in this case do not depend on b_z and are given by

$$E_n = \hbar v_F \pm \sqrt{2eBn + k_x^2}.$$

Furthermore, we found that the lowest Landau level is spin-polarized in the x-direction, but the higher Landau levels are not.

Next, in Chapter 3, we used the solutions we found in Chapter 2 to construct surface states on a half-infinite Weyl semimetal. We found the wave function in the bulk and vacuum, and proceeded to match them at the boundary. The surface states were first derived for zero magnetic field. We found gapless, chiral surface states with dispersion $E = -v_F k_y$, existing on the Fermi arc $|k_z| < b_z$. We continued by adding the effect of the Rashba spin-orbit term due to an external electric field $\mathbf{E}$, following Ref. [1]. For an electric field parallel to the surface $\mathbf{E} = E_z \hat{z}$, we found that the linearity of the zero magnetic field dispersion and the Fermi arc are preserved, but that the Fermi velocity is rescaled by a factor $\sqrt{1 + E_z^2}$. Interestingly, for an electric field perpendicular to the surface, $\mathbf{E} = E_x \hat{x}$, we found a non-linear dispersion

$$E = -\frac{(1 - E_x)^2 b_z k_y + E_x(k_y^2 + k_z^2 - b_z^2)}{\sqrt{(b_z + E_x k_y)^2 + E_x^2 k_z^2}},$$

which is no longer defined on a straight Fermi arc. Instead, the solution is now only defined in the exterior of the two circles defined by

$$\left(k_y + \frac{b_z}{E_x}\right)^2 + \left(k_z \pm \frac{b_z}{2}(1 + \frac{1}{E_x^2})\right)^2 = \frac{b_z^2}{4}\left(1 + \frac{1}{E_x}\right)^2.$$

Inside these two circles, there are no surface states and the problem corresponds to a topologically trivial insulator. After completing the zero magnetic field section, we continued by looking at low magnetic fields parallel to the surface. Since an exponential ansatz no longer worked, we used a WKB approximation to find solutions, following Ref. [21]. The surface state dispersion turned out to be unaffected, however the decay of the wave function into the semimetal had changed and was no longer the same for every spinor-component. Finally, we looked at a magnetic field perpendicular to the surface. We found the wave functions in the semimetal and vacuum, which are linear combinations of the Landau levels. However, we found that there are no bound states possible in a half-infinite semimetal. Next, we looked at the effects of the anomalous magnetic terms on the surface states we found for a magnetic field parallel to the surface. The Zeeman term gave a shift $b_z \to b_z + \mu_2 B$, widening the Fermi arc, but did not affect the energy. The tilt term vastly changed the dispersion and the allowed region in momentum space. We found the new dispersion

$$E = \mu_1 B b_z \left(1 - \frac{k_z^2}{b_z^2}\right) - k_y \sqrt{1 - (\mu_1 B)^2 \frac{k_z^2}{b_z^2}},$$

which now depends on b_z and k_z. The allowed region in momentum space is bounded by two hyperbolic curves defined by

$$k_y = \frac{k_z \pm b_z}{\mu_1 B k_z} \sqrt{b_z^2 - (\mu_1 B k_z)^2}.$$

The Fermi arcs are therefore no longer straight lines. Combining the two effects shifts $b_z \to b_z + \mu_2 B$ in the above results, causing the dispersion to also depend on μ_2.

Since we found no surface state solutions in a half-infinite semimetal for a magnetic field perpendicular to the surface, in Chapter 4 we looked at surface states on a finite slab of semimetal. We found that bound solutions were possible, but were difficult to find. Since the energy spacing is small for low magnetic fields, we could not limit the matching procedure to just a few Landau levels, causing the problem to be unsolvable analytically. However, we noticed that in the high magnetic field limit we can neglect all Landau levels except the lowest one, allowing us to solve the problem. We found that closed magnetic orbits are possible due to the lowest chiral Landau level propagating through the bulk. The lowest Landau level acts as a one-way "conveyor belt", carrying particles from one surface to the other. These orbits have discrete energy levels, which for $m \to \infty$ in the vacuum become

$$E = \frac{\hbar v_F (q + \frac{1}{2})\pi}{L},$$

where q is a integer ranging from $(-\infty, \infty)$. We looked at anomalous effects on these orbits and found that the Fermi momentum is rescaled and the energy is

Zeeman shifted, resulting in

$$E = \frac{(\hbar v_F + \mu_1 B)(q + \frac{1}{2})\pi}{L} + \mu_2 B$$

Finally, we found an approximation of the first-order correction in B on this result by adding one more Landau level, and found the energy levels

$$E = \frac{\hbar v_F \left(q + \frac{1}{2}(1 + \frac{b_z \hbar}{eBL})\right)\pi}{L + \frac{b_z \hbar}{eB}}.$$

We argued that the approximation could be improved by adding more Landau levels, but concluded that this is the main contribution to the first-order correction in B to the energy.

5.2 Outlook

To conclude, we have found the behaviour of the surface states in a Weyl semimetal under influence of a magnetic field. We were able to treat almost all cases, parallel and perpendicular magnetic fields, in the high magnetic field limit and low magnetic field limit. We were also able to find the effects of the unusually large anomalous magnetic moment of Weyl semimetals. Therefore, this research is almost complete. A few more points could be looked at further to fully understand this topic. For one, the behaviour of the surface states for a perpendicular low magnetic field is not known. Using our method, we could not find solutions to this problem. However, there may be other methods one could use that do not require all Landau levels to be taken into account. Furthermore, in Chapter 4 we looked at the corrections to the energy by adding one Landau level. Adding another Landau level may increase numerical complexity, but can be done. This might give a more accurate first order correction in B to the energy. Another point which would give a more complete picture, is finding the corrections of the first Landau level while adding the anomalous terms. This may change the first-order corrections in B slightly, as the anomalous terms affect the first Landau level as well.

Chapter 6

Appendix A1

6.1 Appendix A: Harmonic oscillator wavefunctions with splitting of cones

The harmonic oscillator ladder operators without the splitting of the cones are given by

$$a = \frac{1}{\sqrt{2eB}} \left[-i\partial_z - i(eBz + k_y) \right], \tag{6.1}$$

$$a^\dagger = \frac{1}{\sqrt{2eB}} \left[-i\partial_z + i(eBz + k_y) \right]. \tag{6.2}$$

The ground state is given by the solution of $a\,|0\rangle = 0$. The solutions of this differential equation are given by

$$|0\rangle = \psi_0(z) = \sqrt{\frac{eB}{\pi}} e^{-\frac{(eBz+k_y)^2}{2eB}}. \tag{6.3}$$

Higher level states are obtained by iteratively applying the raising operator $a^\dagger$. In general the n-th level state is given by

$$\psi_n(z) = \frac{i^n}{\sqrt{2^n n!}} \left(\frac{eB}{\pi} \right)^{1/4} e^{-\frac{(eBz+k_y)^2}{2eB}} H_n\left(\frac{1}{\sqrt{eB}} (eBz + k_y) \right), \tag{6.4}$$

where $H_n(x)$ are Hermite polynomials. We add the splitting of the cones in the Hamiltonian by shifting $\mathbf{k} \to \mathbf{k} - \epsilon b_z \hat{z}$. This results in adding $-\epsilon b_z \sigma_3$ to the Hamiltonian. In turn this requires us to redefine the ladder operators in order to diagonalize the Hamiltonian. The new ladder operators are given by

$$a = \frac{1}{\sqrt{2eB}} \left[-i\partial_z - i(eBz + k_y) - \epsilon b_z \right]$$

$$a^\dagger = \frac{1}{\sqrt{2eB}} \left[-i\partial_z + i(eBz + k_y) - \epsilon b_z \right].$$

We need to make slight adjustments to the ground-state wave function to still satisfy $a\,|0\rangle = 0$. We need to cancel the ϵb_z term to get 0 again, so we add a factor $\epsilon i b_z z$ in the exponential.

$$\begin{aligned} a\,|0\rangle &= \frac{1}{\sqrt{2eB}} \left(-i\partial_z - i(eBz + k_y) - \epsilon b_z \right) \left(\frac{eB}{\pi} \right)^{1/4} \quad e^{i\epsilon b_z z} \quad e^{-\frac{(eBz+k_y)^2}{2eB}} \\ &= \frac{1}{\sqrt{2}} \left(\frac{1}{eB\pi} \right)^{1/4} \left(\epsilon b_z + \frac{2i(eBz + k_y)eB}{2eB} - i(eBz + k_y) - \epsilon b_z \right) e^{i\epsilon b_z z} \quad e^{-\frac{(eBz+k_y)^2}{2eB}} \\ &= 0 \end{aligned}$$

So the new ground state is given by

$$\psi_0(z) = \left(\frac{eB}{\pi}\right)^{1/4} e^{i\epsilon b_z z} e^{-\frac{(eBz+k_y)^2}{2eB}}. \tag{6.5}$$

The phase is added to all the excited states as well. We can see this by calculating some excited states. The first excited state is given by

$$\begin{aligned}
\psi_1(z) = a^\dagger \psi_0(x) &= \frac{1}{\sqrt{2eB}} \left[-i\partial_z + i(eBz + k_y) - \epsilon b_z\right] \psi_0(z) \\
&= \frac{1}{\sqrt{2}} \left(\frac{1}{eB\pi}\right)^{1/4} \left(\epsilon b_z + \frac{2i(eBz + k_y)}{2eB} + i(eBz + k_y) - \epsilon b_z\right) e^{i\epsilon b_z z} e^{-\frac{(eBz+k_y)^2}{2eB}} \\
&= \frac{2}{\sqrt{2}} \left(\frac{1}{eB\pi}\right)^{1/4} i(eBz + k_y) e^{i\epsilon b_z z} e^{-\frac{(eBz+k_y)^2}{2eB}} \\
&= \frac{2i}{\sqrt{2}} \frac{(eBz + k_y)}{\sqrt{eB}} \psi_0(z) = \frac{i}{\sqrt{2}} H_1\left(\frac{1}{\sqrt{eB}}(eBz + k_y)\right) \psi_0(z).
\end{aligned}$$

When we look at terms involving ϵb_z in the Hermite polynomials we see that they are always canceled. Therefore the only b_z dependence in higher level states is in $\psi_0(z)$. This means that the new states are simply the old states multiplied by the phase $e^{\epsilon i b_z z}$.

6.2 Appendix B: First-order perturbation theory

We check the first order correction on the wavefunction to see if we can reproduce the phase shift $e^{ib_x x}$. So up to first order we expect the wavefunction to have a correction of $ib_x x$.

We started with the Hamiltonian

$$H = \epsilon v_F \begin{pmatrix} k_z & -i\frac{\partial}{\partial x} + i(eBx - k_y) \\ -i\frac{\partial}{\partial x} - i(eBx - k_y) & -k_z \end{pmatrix},$$

which we rewrote in terms of the ladder operators $a, a^\dagger$, giving

$$H = \epsilon \begin{pmatrix} -v_F k_z & -\beta a^\dagger \\ -\beta a & v_F k_z \end{pmatrix},$$

where $\beta = v_F\sqrt{2eB}$. Solving the Schrödinger equation gave us the energies $E_n = \pm\sqrt{v_F^2 k_z^2 + \beta^2 n}$, with the special case $n = 0$ having energy $E_0 = +v_f k_z$. For $n \neq 0$ the eigenstates are given by

$$|\psi_n\rangle = \begin{pmatrix} a_n |n\rangle \\ b_n |n-1\rangle \end{pmatrix},$$

where

$$\begin{aligned} a_n &= \frac{1}{\sqrt{2}}\left[1 + \frac{v_F^2 k_z^2 + v_F k_z E_n}{\beta^2 n}\right], \\ b_n &= -\frac{E_n + v_F k_z}{\beta\sqrt{n}} a_n. \end{aligned}$$

For $n = 0$ the eigenstate is $|\psi_0\rangle = \begin{pmatrix} |0\rangle \\ 0 \end{pmatrix}$. The first order correction to the wave function is given by

$$|\psi_n^{(1)}\rangle = \sum_{k\neq n} \frac{1}{E_n - E_k} \langle\psi_k^{(0)}| \begin{pmatrix} 0 & v_F b_x \\ v_F b_x & 0 \end{pmatrix} |\psi_n^{(0)}\rangle \, |\psi_k^{(0)}\rangle .$$

For $n \neq 0$ this is given by

$$\begin{aligned} |\psi_n^{(1)}\rangle &= \sum_{k\neq n} \frac{1}{E_{n,k}} \begin{pmatrix} a_k \langle k| \\ b_k \langle k-1| \end{pmatrix}^T \begin{pmatrix} b_x b_n |n-1\rangle \\ b_x a_n |n\rangle \end{pmatrix} \\ &= \frac{v_F b_x}{E_{n,n+1}} a_n b_{n+1} |\psi_{n+1}^{(0)}\rangle + \frac{v_F b_x}{E_{n,n-1}} a_{n-1} b_n |\psi_{n-1}^{(0)}\rangle . \end{aligned}$$

For $n = 0$ we get

$$|\psi_0^{(1)}\rangle = \frac{v_F b_x}{E_{0,1}} a_0 b_1.$$

Now we want to compare this to the first order correction $|\psi_n^{(1)}\rangle = ib_x x \mathbf{1}_2 |\psi_n^{(0)}\rangle$. Recall that our ladder operators were given by

$$\begin{aligned} a &= \alpha\left[p_x - i(eBx - k_y)\right], \\ a^\dagger &= \alpha\left[p_x + i(eBx - k_y)\right], \end{aligned}$$

where $\alpha = \frac{1}{\sqrt{2eB}}$. So we can express x as $x = i\alpha(a - a^\dagger) + 2\alpha^2 k_y$. We discard the constant k_y term since this is just a shift in x. We get

$$\begin{aligned} ib_x x \mathbf{1}_2 \left|\psi_n^{(0)}\right\rangle &= \begin{pmatrix} ib_x i\alpha(a-a^\dagger) & 0 \\ 0 & ib_x i\alpha(a-a^\dagger) \end{pmatrix} \begin{pmatrix} a_n \left|n\right\rangle \\ b_n \left|n-1\right\rangle \end{pmatrix} \\ &= -b_x\alpha \begin{pmatrix} a_n\left(\sqrt{n}\left|n-1\right\rangle - \sqrt{n+1}\left|n+1\right\rangle\right) \\ b_n\left(\sqrt{n-1}\left|n-2\right\rangle - \sqrt{n}\left|n\right\rangle\right) \end{pmatrix}. \end{aligned}$$

It is clear that this is a superposition of $\left|\psi_{n+1}^{(0)}\right\rangle$ and $\left|\psi_{n-1}^{(0)}\right\rangle$. We can project from the left with $\left\langle\psi_{n+1}^{(0)}\right|$ to find the coefficient belonging to that term, giving

$$\begin{aligned} \left\langle\psi_{n+1}^{(0)}\right| ib_x x \mathbf{1}_2 \left|\psi_n^{(0)}\right\rangle &= -b_x\alpha \begin{pmatrix} a_{n+1}\left\langle n+1\right| \\ b_{n+1}\left\langle n\right| \end{pmatrix}^T \begin{pmatrix} a_n\left(\sqrt{n}\left|n-1\right\rangle - \sqrt{n+1}\left|n+1\right\rangle\right) \\ b_n\left(\sqrt{n-1}\left|n-2\right\rangle - \sqrt{n}\left|n\right\rangle\right) \end{pmatrix} \\ &= -b_x\alpha\left[-a_n a_{n+1}\sqrt{n+1} - b_n b_{n+1}\sqrt{n}\right]. \end{aligned}$$

The coefficient we got from first order perturbation theory was $\frac{b_x v_F}{E_{n,n+1}} a_n b_{n+1}$. Therefore, we want to rewrite our result in terms of $a_n b_{n+1}$, giving

$$\begin{aligned} \left\langle\psi_{n+1}^{(0)}\right| ib_x x \mathbf{1}_2 \left|\psi_n^{(0)}\right\rangle &= b_x\alpha\left[-a_n b_{n+1}\frac{\beta(n+1)}{E_{n+1}+v_F k_z} - a_n b_{n+1}\frac{E_n + v_F k_z}{\beta}\right] \\ &= b_x v_F a_n b_{n+1}\left[-\frac{n+1}{E_{n+1}+v_F k_z} - \frac{\alpha^2(E_n+v_F k_z)}{v_F^2}\right]. \end{aligned}$$

If the coefficients of the first order perturbation theory and the first order correction of $e^{ib_x x}\left|\psi_n^{(0)}\right\rangle$ are the same, we have

$$\left[-\frac{n+1}{E_{n+1}+v_F k_z} - \frac{\alpha^2(E_n+v_F k_z)}{v_F^2}\right] = \frac{1}{E_n - E_{n+1}}.$$

We can reduce the left hand side to

$$\left[-\frac{n+1}{E_{n+1}+v_F k_z} - \frac{\alpha^2(E_n+v_F k_z)}{v_F^2}\right] = -\frac{1}{v_F}\left(\sqrt{\alpha^4 k_z^2 + \alpha^2(n+1)} + \sqrt{\alpha^4 k_z^2 + \alpha^2 n}\right).$$

We multiply by $(E_n - E_{n+1})$, which should give us 1, giving

$$\begin{aligned} &-\frac{1}{v_F}\left(\sqrt{\alpha^4 k_z^2 + \alpha^2(n+1)} + \sqrt{\alpha^4 k_z^2 + \alpha^2 n}\right)(E_n - E_{n+1}) \\ &= \frac{1}{v_F}\Bigg[-\sqrt{(\alpha^4 k_z^2 + \alpha^2(n+1))(v_F^2 k_z^2 + \beta^2 n)} + \sqrt{(\alpha^4 k_z^2 + \alpha^2(n+1))(v_F^2 k_z^2 + \beta^2(n+1))} \\ &- \sqrt{(\alpha^4 k_z^2 + \alpha^2 n)(v_F^2 k_z^2 + \beta^2 n)} + \sqrt{(\alpha^4 k_z^2 + \alpha^2 n)(v_F^2 k_z^2 + \beta^2(n+1))}\Bigg] \\ &= -\sqrt{(\alpha^2 k_z^2 + n)(\alpha^2 k_z^2 + (n+1))} - (\alpha^2 k_z^2 + n) + (\alpha^2 k_z^2 + (n+1)) + \sqrt{(\alpha^2 k_z^2 + n)(\alpha^2 k_z^2 + (n+1))} \\ &= -(\alpha^2 k_z^2 + n) + (\alpha^2 k_z^2 + (n+1)) \\ &= 1, \end{aligned}$$

which confirmes that the $\left|\psi_{n+1}^{(0)}\right\rangle$ coefficients are the same. We do the same for the $\left|\psi_{n-1}^{(0)}\right\rangle$ component, giving

$$\left\langle\psi_{n-1}^{(0)}\right| ib_x x \mathbf{1}_2 \left|\psi_n^{(0)}\right\rangle = -b_x\alpha\left[a_{n-1}a_n\sqrt{n-1} + b_{n-1}b_n\sqrt{n}\right].$$

We have to compare this to $\frac{b_x v_F}{E_{n,n-1}} a_n b_{n-1}$. So we rewrite in terms of $a_n b_{n-1}$, giving

$$\begin{aligned}\langle \psi_{n-1}^{(0)}| \, ib_x x \mathbf{1}_2 \, |\psi_n^{(0)}\rangle &= b_x v_F a_n b_{n-1} \left(\frac{n-1}{E_{n-1} + v_F k_z} + \frac{\alpha^2 (E_n + v_F k_z)}{v_F^2} \right) \\ &= b_x v_F a_n b_{n-1} \left(\sqrt{\frac{a^2 \left(a^2 k_z^2 + (n-1)\right)}{v^2}} + \sqrt{\frac{a^4 k_z^2 + a^2 n}{v^2}} \right).\end{aligned}$$

In order for the coefficients to be the same, it has to hold that

$$\sqrt{\frac{a^2 \left(a^2 k_z^2 + (n-1)\right)}{v^2}} + \sqrt{\frac{a^4 k_z^2 + a^2 n}{v^2}} = \frac{1}{E_n - E_{n-1}}.$$

We multiply the left hand side by $(E_n - E_{n-1})$, giving

$$\begin{aligned}&\left(\sqrt{\frac{a^4 k_z^2 + \alpha^2 (n-1)}{v^2}} + \sqrt{\frac{a^4 k_z^2 + a^2 n}{v^2}} \right) (E_n - E_{n-1}) \\ &= \sqrt{(\alpha^4 k_z^2 + \alpha^2 (n-1))(k_z^2 + \frac{n}{\alpha^2})} - \sqrt{(\alpha^4 k_z^2 + \alpha^2 (n-1))(k_z^2 + \frac{n-1}{\alpha^2})} \\ &+ \sqrt{(\alpha^4 k_z^2 + \alpha^2 n)(k_z^2 + \frac{n}{\alpha^2})} - \sqrt{(\alpha^4 k_z^2 + \alpha^2 n)(k_z^2 + \frac{n-1}{\alpha^2})} \\ &= -(\alpha^2 k_z^2 + (n-1)) + (\alpha^2 k_z^2 + n) \\ &= 1.\end{aligned}$$

This result confirms the coefficients of $|\psi_{n-1}^{(0)}\rangle$ are also the same. To conclude, we have shown that the first order correction on the wavefunction is consistent with a phase shift $e^{ib_x x}$.

Bibliography

[1] E.C.I. van der Wurff and H.T.C. Stoof. Large anomalous magnetic moment in three-dimensional Dirac and Weyl semimetals. *Phys. Rev.*, B94(155118), 2016.

[2] "Nobelprize.org". Scientific background on the Nobel Prize in physics 2010.

[3] A. H. Castro Neto, F. Guinea, N. M. R. Peres, K. S. Novoselov, and A. K. Geim. The electronic properties of graphene. *Rev. Mod. Phys.*, 81(109-162), 2009.

[4] C.L. Kane and E.J. Mele. Z2 topological order and the quantum spin Hall effect. *Phys. Rev. Lett.*, 95(146802), 2005.

[5] M. Berry. Quantal phase factors accompanying adiabatic changes. *Royal Society Publishing*, 1984.

[6] Robert-Jan Slager Jun-Won Rhim, Jens H. Bardarson. Unified bulk-boundary correspondence for band insulators. *Phys. Rev. B*, 97(115143), 2018.

[7] B. Q. Lv, S.Muff, T. Qian, Z. D. Song, S. M. Nie, N. Xu, P. Richard, C. E. Matt, N. C. Plumb, L. X. Zhao, G. F. Chen, Z. Fang, X. Dai, J. H. Dil, J. Mesot, M. Shi, H. M. Weng, and H. Ding. Observation of Fermi-arc spin texture in TaAs. *Phys. Rev. Lett.*, 115(217601), 2015.

[8] A.A. Burkov. Anomalous Hall effect in Weyl metals. *Phys. Rev. Lett.*, 113(187202), 2014.

[9] S.Y. Xu, I. Belopolski, N. Alidoust, M. Neupane, G. Bian, C. Zhang, R. Sankar, G. Chang, Z. Yuan, C.C. Lee, S.M. Huang, J. Ma H. Zheng, D. S. Sanchez, B. Wang, A. Bansil, F. Chou, P. Shibayev, H. Lin, S. Jia, and M. Z. Hasan. Discovery of a Weyl fermion semimetal and topological Fermi arcs. *Science*, 613, 2015.

[10] B. Q. Lv, H. M. Weng, B. B. Fu, X. P. Wang, H. Miao, P. Richard J. Ma, X. C. Huang, L. X. Zhao, G. F. Chen, Z. Fang, T. Qian X. Dai, and H. Ding. Experimental discovery of Weyl semimetal TaAs. *Phys. Rev.*, 5(031013), 2015.

[11] B. Q. Lv, N. Xu, H. M. Weng, J. Z. Ma, P. Richard, L. X. Zhao X. C. Huang, G. F. Chen, C. E. Matt, F. Bisti, V. N. Strocov, J. Mesot, Z. Fang, X. Dai, T. Qian, M. Shi, and H. Ding. Observation of Weyl nodes in TaAs. *Nature Physics*, 11(724), 2015.

[12] Shin-Ming Huang, Su-Yang Xu, Ilya Belopolski, Chi-Cheng Lee, Guoqing Chang, BaoKai Wang, Nasser Alidoust, Guang Bian, Madhab Neupane, Chenglong Zhang, Shuang Jia, Arun Bansil, Hsin Lin, and M. Zahid Hasan. A Weyl fermion semimetal with surface Fermi arcs in the transition metal monopnictide TaAs class. *Nature Communications*, 6(7373), 2015.

[13] S.Y. Xu, N. Alidoust, I. Belopolski, Z. Yuan, G. Bian, T.R. Chang, H. Zheng, V. N. Strocov, G. Chang D. S. Sanchez, C. Zhang, D. Mou, Y. Wu, L. Huang, C.-C. Lee, S.-M. Huang, B. Wang, A. Bansil, H.T. Jeng, T. Neupert, A. Kaminski, H. Lin, S. Jia, and M. Z. Hasan. Discovery of a Weyl fermion state with Fermi arcs in Niobium Arsenide. *Nature Physics*, 11(748), 2015.

[14] S.Y. Xu, I. Belopolski, D. S. Sanchez, C. Zhang, G. Chang, C. Guo, G. Bian, Z. Yuan, H. Lu, T.R. Chang, P. P. Shibayev, M. L. Prokopovych, N. Alidoust, H. Zheng, C.C. Lee, S.-M. Huang, R. Sankar, F. Chou, C.H. Hsu, H.-T. Jeng, A. Bansil, T. Neupert, V. N. Strocov, H. Lin, S. Jia, and M. Z. Hasan. Experimental discovery of a topological Weyl semimetal state in TaP. *Science Adv.*, 1(1501092), 2015.

[15] Ling Lu, Zhiyu Wang, Dexin Ye, Lixin Ran, Liang Fu, John D. Joannopoulos, and Marin Soljacic. Experimental observation of Weyl points. *Science*, 349(6248), 2015.

[16] J Jiang, Z K. Liu, Y Sun, YANG Haifeng, R Rajamathi, Y P. Qi, L X. Yang, C Chen, Han Peng, C Hwang, S Z. Sun, Sung-Kwan Mo, Ivana Vobornik, J Fujii, Stuart Parkin, Claudia Felser, Binghai Yan, and Y L. Chen. Observation of the type-II Weyl semimetal phase in MoTe2. *Nature Communications*, 8(13973), 2017.

[17] Nitesh Kumar1, Yan Sun, Nan Xu, Kaustuv Manna, Mengyu Yao, Vicky Süss1, Inge Leermakers, Olga Young, Tobias Förster, Marcus Schmidt, Horst Borrmann, Binghai Yan, Uli Zeitler, Ming Shi, Claudia Felser, and Chandra Shekhar. Extremely high magnetoresistance andconductivity in the type-II Weyl semimetals WP2 and MoP2. *Nature Communications*, 8(1642), 2017.

[18] J. E. Nafe, E. B. Nelson, and I. I. Rabi. The hyperfine structure of atomic Hydrogen and Deuterium. *Phys. Rev.*, 71(914), 1947.

[19] Julian Schwinger. On quantum-electrodynamics and the magnetic moment of the electron. *Phys. Rev.*, 73(416), 1948.

[20] D. Hanneke, S. Fogwell, and G. Gabrielse. Cavity control of a single-electron quantum cyclotron: Measuring the electron magnetic moment. *Phys.Rev.*, A83(052122), 2011.

[21] Thijs van Gogh. Anomalous magnetic effects in three-dimensional Weyl semimetals. *Utrecht University*, 2017.

[22] Gradshteyn, Izrail Solomonovich, Iosif Moiseevich Ryzhik, Yuri Veniaminovich Geronimus, and Michail Yulyevich Tseytlin. Tables of integrals, series, and products. 1966.

[23] N. Read. Lowest-Landau-level theory of the quantum Hall effect: the Fermi-liquid-like state. *Phys.Rev.*, B58(16262), 1998.

[24] Alexis G. Morris and David L. Feder. Validity of the lowest Landau level approximation for rotating Bose gases. *Phys.Rev.*, A74(033605), 2006.

[25] Andrew C. Potter, Itamar Kimchi, and Ashvin Vishwanath. Quantum oscillations from surface Fermi-arcs in Weyl and Dirac semi-metals. *Nature Communications*, (5161), 2014.

[26] Akira Igarashi and Mikito Koshino. Magnetotransport in Weyl semimetal nanowires. *Phys Rev.*, B95(195306), 2017.

[27] Hao Zheng and M. Zahid Hassan. Quasiparticle interference on type-I and type-II Weyl semimetal surfaces: a review. *Advances in Physics*, X3(1466661), 2018.

[28] Alexey A. Soluyanov, Dominik Gresch, Zhijun Wang, QuanSheng Wu, Matthias Troyer, Xi Dai, and B. Andrei Bernevig. Type-II Weyl semimetals. *Nature*, 527(495-498), 2015.